389741-1-T

THE UNIVERSITY OF MICHIGAN

COLLEGE OF ENGINEERING

DEPARTMENT OF ELECTRICAL ENGINEERING & COMPUTER SCIENCE

Radiation Laboratory

SCATTERING BY GAPS AND CRACKS

Thomas B.A. Senior
John L. Volakis
Radiation Laboratory
Department of Electrical Engineering
and Computer Science
The University of Michigan
Ann Arbor, MI 48109

November, 1988

McDonnell Aircraft Company
St. Louis, MO 63166

Ann Arbor, Michigan

Abstract

A matter of increasing concern in radar scattering is the contribution from gaps and cracks where two component structures come together. For the two-dimensional problem of a narrow gap filled with a resistive or impedance material in an otherwise perfectly conducting plane, the integral equations for the currents induced in the gap are approximated under the assumption that $w << \lambda$, where w is the gap width and λ is the wavelength. The resulting equations are analogous to those occuring in airfoil theory. Exact solutions are derived in special cases and these are used to guide the development of approximate analytical expressions for the diffracted fields which are valid for almost all resistivities of the gap material. By comparison with data obtained from a moment method solution of the problem, it is demonstrated that the results are accurate even for gap widths as large as $\lambda/8$ for H-polarization and $\lambda/4$ for E-polarization, and the application of these formulas to realistic gap geometries is also discussed.

Preface

The body of this report is a paper which has been accepted for publication in the IEEE Transactions on Antennas and Propagation. The determination of the impedance presented by a variety of crack geometries was carried out by Mr. S. M. Kilberg and is described in Appendix A, and the extension to an impedance surface is discussed in Appendix B.

1. Introduction

With the increasing sophistication of radar cross section reduction techniques, gaps and cracks where two component structures come together can become a dominant contributor to the bistatic scattering behavior of a target. In those cases where it is impossible to eliminate the break, it is important to examine the effect of different gap geometries and material inserts, and to develop ways to compute the scattering. For a simple gap whose width w is comparable to or larger than the wavelength λ, consisting of a lossy material insert in an otherwise perfectly conducting plane, the scattered field can be deduced from the GTD solution for an isolated resistive strip [1], or computed using one of the available codes [2] for solving the integral equation for the strip. On the other hand, if $w << \lambda$ (the usual situation at microwave frequencies) an alternative approach is possible, and this is the subject of the present report.

The problem initially considered is that of a two-dimensional slit in a perfectly conducting plane occupied by a resistive material of uniform resistivity R ohms per square and illuminated by a plane wave either H or E polarized. Using Babinet's principle, the integral equations for the currents supported by the material are deduced from the corresponding integral equations for a strip, and then approximated under the assumption that the strip width is small. The resulting equations are special cases of a general airfoil equation, and analytical solutions are derived in the limits of large and small resistivities. Guided by these, and using numerical data obtained from a moment method solution of the equations, approximate analytical expressions for the far zone diffracted field of the gap are developed. These are valid for almost all (complex) resistivities, and their accuracy is verified for gap widths as large as $\lambda/8$ for H-polarization and $\lambda/4$ for E-polarization.

If, instead, the gap is occupied by a material at which an impedance boundary condition is imposed, the analysis is still applicable if R is replaced by $\eta/2$, where η is the surface impedance. Using a quasi-static method we can determine the impedance presented by a gap of almost any configuration, and two examples are given.

2. Integral Equations for a Resistive Insert

A resistive sheet of uniform resistivity R ohms per square occupies the portion $-w/2 < x < w/2$, $-\infty < z < \infty$ of the otherwise perfectly conducting plane $y = 0$. A plane wave is incident on the surface from above (see Figure 1) and we consider separately the case of H- or E-polarization with

$$\bar{H}^i \text{ (or } \bar{E}^i) = \hat{z}\, e^{-ik(x\cos\phi_o + y\sin\phi_o)} \tag{1}$$

respectively, where a time factor $e^{-i\omega t}$ has been assumed and suppressed. In the far zone, the diffracted field attributable to the resistive insert is

$$\bar{H}^d \text{ (or } \bar{E}^d) = \hat{z}\sqrt{\frac{2}{\pi k\rho}}\, e^{i(k\rho - \frac{\pi}{4})} P_{H,E}(\phi, \phi_o) \tag{2}$$

where (ρ, ϕ) are the usual cylindrical coordinates of the obervation point and the task is to determine $P_{H,E}$ under the assumption that $kw << 1$.

2.1 H-Polarization

From Babinet's principle [3] the problem is equivalent to the diffraction of an E polarized plane wave by the complementary resistive strip of resistivity $R' = Z^2/(4R)$ ohms per square where Z is the intrinsic impedance of free space. It is therefore a trivial matter to deduce the integral equation for the current supported by the insert from the integral equation for the strip. Thus [4]

$$\frac{kZ}{4}\int_{-\frac{w}{2}}^{\frac{w}{2}} J_z(x')\, H_o^{(1)}(k|x' - x|)\, dx' = e^{-ikx\cos\phi_o} - R'J_z(x) \tag{3}$$

or $-w/2 < x < w/2$, and in terms of $J_z(x)$

$$P_H(\phi, \phi_o) = -\frac{kZ}{4} \int_{-\frac{w}{2}}^{\frac{w}{2}} J_z(x') e^{-ikx'\cos\phi} dx'. \tag{4}$$

It is now convenient to introduce the new variables

$$\zeta = \frac{2}{w} x, \quad \zeta' = \frac{2}{w} x' \tag{5}$$

and

$$J_1(\zeta) = \frac{ikw}{4} Z J_z(x). \tag{6}$$

Equations (3) and (4) then become

$$-\frac{i}{2} \int_{-1}^{1} J_1(\zeta') H_o^{(1)}\left(\frac{kw}{2} |\zeta - \zeta'|\right) d\zeta' = e^{-i\frac{kw}{2}\zeta\cos\phi_o} + a J_1(\zeta) \tag{7}$$

or $-1 < \zeta < 1$ and

$$P_H(\phi, \phi_o) = \frac{i}{2} \int_{-1}^{1} J_1(\zeta') e^{-i\frac{kw}{2}\zeta'\cos\phi} d\zeta' \tag{8}$$

with

$$a = \frac{4i}{kw} \frac{R'}{Z} = \frac{i}{kw} \frac{Z}{R} . \tag{9}$$

We observe that if R is finite, $a \to \infty$ as $kw \to 0$.

The small argument expansion of the Hankel function is

$$H_o^{(1)}(z) = \frac{2i}{\pi} \left(\ln \frac{z}{2} + \gamma - \frac{i\pi}{2}\right) + 0\left(z^2, z^2 \ln z\right)$$

where $\gamma = 0.5772157....$ is Euler's constant, and hence

$$H_o^{(1)}\left(\frac{kw}{2}\,|\,\zeta' - \zeta\,|\right) = \frac{2i}{\pi}\left(\ln|\,\zeta' - \zeta\,| + A\right) + 0\left\{\left(\frac{kw}{2}\right)^2, \left(\frac{kw}{2}\right)^2 \ln\frac{kw}{2}\right\} \tag{10}$$

with

$$A = \ln\frac{kw}{4} + \gamma - i\frac{\pi}{2}\ . \tag{11}$$

When this is inserted into (7), the lowest order approximation for small kw is

$$\frac{1}{\pi}\int_{-1}^{1} J_1(\zeta')\left\{\ln|\,\zeta' - \zeta\,| + A\right\} d\zeta' = 1 + a\,J_1(\zeta), \tag{12}$$

and (8) becomes

$$P_H(\phi, \phi_o) = \frac{i}{2}\int_{-1}^{1} J_1(\zeta')\,d\zeta'. \tag{13}$$

A further simplification is to write

$$J_1(\zeta) = \left\{1 + \frac{2i}{\pi}AP_H(\phi, \phi_o)\right\}J_2(\zeta)\,,$$

and the integral equation for $J_2(\zeta)$ is then

$$\frac{1}{\pi}\int_{-1}^{1} J_2(\zeta')\ln|\,\zeta' - \zeta\,|\,d\zeta' = 1 + a\,J_2(\zeta) \tag{14}$$

with

$$P_H(\phi, \phi_o) = \frac{i}{2}\left\{1 + \frac{A}{\pi}\int_{-1}^{1} J_2(\zeta')\,d\zeta'\right\}^{-1}\int_{-1}^{1} J_2(\zeta')\,d\zeta'\ . \tag{15}$$

We note that $P_H(\phi, \phi_o)$ depends only on the average value of $J_2(\zeta)$ and is independent of ϕ and ϕ_o. The solution of (14) is discussed in Section 3.

2.2 E-Polarization

If the plane wave incident on the surface y = 0 is E polarized, the integral equation for the current supported by the insert is, from Babinet's principle,

$$\frac{1}{4k}\left(k^2+\frac{\partial^2}{\partial x^2}\right)\int_{-\frac{w}{2}}^{\frac{w}{2}} J_x(x')\,H_o^{(1)}(k\,|x'-x|)\,dx' = \sin\phi_o\, e^{-ikx\cos\phi_o} - \frac{R'}{Z}J_x(x) \qquad (16)$$

[see 5] valid for - w/2 < x < w/2 with $J_x(\pm w/2) = 0$, and the diffracted far field amplitude is

$$P_E(\phi,\phi_o) = \frac{k}{4}\sin\phi \int_{-\frac{w}{2}}^{\frac{w}{2}} J_x(x')\,e^{-ikx'\cos\phi}\,dx'. \qquad (17)$$

It is now convenient to write

$$J_3(\zeta) = \frac{i}{kw\sin\phi_o}J_x(x)\ , \qquad (18)$$

where ζ and ζ' are the variables defined in (5). Equation (16) then becomes

$$\left\{\frac{\partial^2}{\partial\zeta^2}+\left(\frac{kw}{2}\right)^2\right\}\frac{1}{2i}\int_{-1}^{1} J_3(\zeta')\,H_0^{(1)}\left(\frac{kw}{z}|\zeta'-\zeta|\right)d\zeta' = e^{-i\frac{kw}{2}\zeta\cos\phi_o} - b\,J_3(\zeta) \qquad (19)$$

for $-1 < \zeta < 1$ with

$$J_3(\pm 1) = 0 \qquad (20)$$

and

$$b = -ikw\frac{R'}{Z} = -\frac{ikw}{4}\frac{Z}{R}\ . \qquad (21)$$

We observe that if $R \neq 0$, $b \to 0$ as $kw \to 0$, and in terms of $J_3(\zeta)$

$$P_E(\phi, \phi_o) = -i \frac{(kw)^2}{8} \sin\phi \sin\phi_o \int_{-1}^{1} J_3(\zeta') e^{-i\frac{kw}{2}\zeta' \cos\phi} d\zeta'. \quad (22)$$

When the small argument expansion of the Hankel function is inserted into (19), the lowest order approximation for small kw is

$$\frac{\partial^2}{\partial\zeta^2} \frac{1}{\pi} \int_{-1}^{1} J_3(\zeta') \ln|\zeta' - \zeta| d\zeta' = 1 - b J_3(\zeta) \quad . \quad (23)$$

Also

$$P_E(\phi, \phi_o) = -i \frac{(kw)^2}{8} \sin\phi \sin\phi_o \int_{-1}^{1} J_3(\zeta') d\zeta' \quad , \quad (24)$$

and since $J_3(\zeta)$ is independent of ϕ and ϕ_o, the only angular dependence of $P_E(\phi, \phi_o)$ is that shown explicitly in (24). The determination of $J_3(\zeta)$ as a function of b is addressed in the next section.

3. Solution of the Integral Equations

The integral equations (14) and (23) are closely related to equations which occur in airfoil theory. If (14) is differentiated with respect to ζ we obtain

$$a J_2'(\zeta) + \frac{1}{\pi} \int_{-1}^{1*} J_2(\zeta') \frac{d\zeta'}{\zeta' - \zeta} = 0 \quad (25)$$

where the prime attached to the function indicates the derivative and the asterisk denotes the Cauchy principal value. Similarly, by carrying out the differentiation in (23) and invoking (20), the equation can be written as

$$b\,J_3(\zeta) - \frac{1}{\pi}\int_{-1}^{1}{}^{*} J_3'(\zeta')\,\frac{d\zeta'}{\zeta' - \zeta} = 1 \ . \qquad (26)$$

Both are examples of a general equation whose reduction to a regular Fredholm equation can be achieved [6] using a Hilbert transform, but unfortunately a closed-form analytical solution is not available. On the other hand, the dominant terms for |a|, |b| small or large compared with unity are easily obtained. When used in conjunction with numerical solutions of (14) and (23), these suggest expressions for the far field amplitudes which are valid for (almost) all a and b.

3.1 Determination of $P_H(\phi, \phi_o)$

Since P_H is independent of ϕ and ϕ_o but is expected to be a function of a, we shall henceforth write it as $P_H(a)$ and in terms of

$$K_H(a) = \frac{1}{\pi}\int_{-1}^{1} J_2(\zeta')\,d\zeta' \qquad (27)$$

we have (see (15))

$$P_H(a) = \frac{i\pi}{2} K_H(a)\,\{\,1 + AK_H(a)\,\}^{-1} \qquad (28)$$

For a = 0, corresponding to an open slit, $J_2(\zeta)$ can be obtained from (25) using a Hilbert transform [7] or, alternatively, from (14) using the inversion formulas in [8]. The result is

$$J_2(\zeta) = -\frac{1}{\ell n 2}\sqrt{1 - \zeta^2}$$

giving

$$K_H(0) = -\frac{1}{\ell n 2} \quad . \tag{29}$$

Hence

$$P_H(0) = \frac{i\pi}{2B} \tag{30}$$

where

$$J_2(\zeta) \cong -\frac{1}{a}$$

implying

$$K_H(a) \cong -\frac{2}{\pi a} \quad , \tag{32}$$

and an expression for K_H (a) which encompasses (29) and (32) is

$$K_H(a) = -\left\{ \frac{\pi a}{2} + \ell n\, 2 + f(a) \right\}^{-1} \tag{33}$$

provided f(0) = 0 and f(a) = 0 (a^{ε}) for large |a| with $\varepsilon < 1$.

To determine f(a), a program was written to solve the integral equation (14) by the moment method. From the resulting data for K_H (a) it was found that f(a) has dominant simple poles at a = -0.15, -0.29 and zeros at a = 0, -0.20, and an expression for f(a) consistent with this is

$$f(a) = \frac{c\,a\,(a + 0.20)}{(a + 0.15)\,(a + 0.29)} \tag{34}$$

In (34) c is a constant which was found from a numerical examination of K_H (a) for negative real a. As shown in Figure 2, K_H (a) has simple poles at a = -0.25 and -0.56, and both specify c = 0.10. An approximate formula for K_H (a) is therefore*

$$K_H(a) = -\frac{(a + 0.15)\,(a + 0.29)}{(\frac{\pi a}{2} + \ell n\, 2)\,(a + 0.15)\,(a + 0.29) + 0.10a\,(a + 0.20)} \tag{35}$$

and when this is substituted into (28), an explicit analytical expression for P_H (a) is obtained.

The values of K_H (a) predicted by (35) have been compared with the moment method data as a function of |a| for a variety of arg a. With the possible exception of negative real a in the range -0.1 < a < 0, the agreement is excellent for all a and, in particular, the magnitude is in error by less than one percent for |a| < 10.

3.2 Determination of $P_E(\phi, \phi_o)$

The procedure employed is similar to that for H-polarization. Writing

$$K_E(b) = \frac{1}{\pi}\int_{-1}^{1} J_3(\zeta')\,d\zeta' \tag{36}$$

we have (see (24))

$$P_E(\phi, \phi_o) = -\frac{i\pi}{8}(kw)^2 \sin\phi \sin\phi_o\, K_E(b) \tag{37}$$

* Since the kernel of (14) is symmetric, the eigenvalues are all real and the only possible poles of K_H (a) are also real.

where $J_3(\zeta)$ is given by the integral equation (23) or (26).

If $b = 0$, $J_3(\zeta)$ can be obtained from (26) by applying a Hilbert transform or, alternatively, by integrating out the derivatives in (23) and using the inversion formulas [8] in conjunction with (20). The result is

$$J_3(\zeta) = \sqrt{1 - \zeta^2}$$

giving

$$K_E(0) = 0.5, \tag{38}$$

and when this is inserted into (37), the far field amplitude agrees with the known solution [9] for a perfectly conducting strip. On the other hand, if $|b| >> 1$,

$$J_3(\zeta) \cong \frac{1}{b}$$

implying

$$K_E(b) \cong \frac{2}{\pi b}. \tag{39}$$

The limiting values (38) and (39) can now be used to guide the development of an analytical expression for $K_E(b)$.

From the results of a numerical solution of (23) by the moment method, it was found that $K_E(b)$ has a dominant pole at $b = -1.15$ and an infinite series of adjacent poles and zeros at increasingly negative real values of b. The effect of each pole-zero pair is apparent only in the immediate vicinity, and for other values of b an adequate

approximation to K_E (b) is obtained by including only five pole-zero pairs. Consistent with the known value of K_E (0), we derived that

$$K_E(b) = \frac{0.62}{b + 1.15} \cdot \frac{(b + 4.08)(b + 7.26)(b + 10.37)(b + 13.43)(b + 16.46)}{(b + 4.27)(b + 7.37)(b + 10.45)(b + 13.49)(b + 16.50)} \qquad (40)$$

leading to an explicit analytical approximation to $P_E(\phi, \phi_o)$.

To assess the accuracy of (40), the results were compared with moment method data as a function of |b| for various arg (b). The agreement was good. For |b| < 10 the amplitudes differed by less than 1.5 percent, and for non-negative-real b the error was less than 2 percent out to |b| = 100. Because of the manner in which b depends on kw (see (21)), the smaller values of |b| are more important for practical purposes.

4. Verification and Extension of the Theory

The preceeding analyses are based on a low frequency approximation to the integrals and, as such, can be justified only for electrically narrow gaps. In practice, however, the expressions for $P_{H,E}(\phi, \phi_o)$ are accurate for a significant range of gap widths, and this has been verified by comparing the results with those generated by a moment method solution of (3) and (16). The particular code employed [2] computes the matrix elements using an analytical expression for all cells within a fraction of a wavelength of each other, thereby avoiding the errors common to many moment method codes when applied to small structures.

In Figures 3 through 8 the scattering length (or scattering cross section per unit length in the z direction)

$$\sigma_{H,E}(\phi, \phi_o) = \frac{2\lambda}{\pi} |P_{H,E}(\phi, \phi_o)|^2 \qquad (41)$$

computed using the code is compared with the values predicted by (28) and (37) for a variety of R as a function of kw. For E-polarization (Figures 3-5) the agreement is good

out to kw ≅ 1.6 almost independently of ϕ and ϕ_0, and the same is true for the phase of P_E. With H-polarization, however, the low frequency solution does not depend on ϕ and ϕ_0 whereas the exact solution does to an increasing extent as kw increases. This is evident from Figures 6-8 where the vertical lines show the total variations of the moment method data for $\sigma_H(\phi, \phi_0)$ over the range $0 < \phi \leq 90°$ in the case of backscattering ($\phi_0 = \phi$). The agreement with the low frequency solution is now good out to kw ≅ 0.8 with a similar result for the phase.

For an actual gap in an airframe structure, an insert composed of a resistive sheet material is not a very realistic model, but the analyses is also applicable to another type of insert. If the insert consists of a material satisfying an impedance boundary condition at the surface y = 0, - w/2 < x < w/2, there is no Babinet equivalent problem, but it is still possible to derive an integral equation for the (magnetic) current supported by the insert by using a half-space Green's function in conjunction with a standard integral representation of the field in y ≥ 0. The resulting equations are identical to (3) and (16) with R replaced by $\eta/2$ where η is the surface impedance. Thus

$$a = \frac{2i}{kw}\frac{Z}{\eta}, \quad b = -\frac{ikw}{2}\frac{Z}{\eta}, \tag{42}$$

and with this identification, the expressions (28) and (37) for the far field amplitudes are immediately applicable.

A particular advantage of this generalization is that for an actual structure the impedance can be determined experimentally or, for a narrow gap of relatively simple geometry, using a quasi-static analysis or code. As an example, consider the cavity-backed slot shown in Figure 9(a). If $w << \lambda$ and the relative permittivity and permeability of the material filling the cavity are ε' and μ', respectively, the lowest order mode field within the cavity when an H polarized plane wave is incident can be written as

$$H_z = \cos\{pk(y+d)\}$$

with

$$E_x = -\frac{Z}{ik\varepsilon'}\frac{\partial H_z}{\partial y}, \quad E_y = \frac{Z}{ik\varepsilon'}\frac{\partial H_z}{\partial x}$$

where

$$p = \sqrt{\varepsilon'\mu'} \tag{43}$$

s the refractive index of the material. From the continuity of the tangential fields at the surface y = 0 it now follows that

$$\eta = -\frac{iZp}{\varepsilon'}\tan(pkd) \tag{44}$$

Similarly, for E-polarization, the lowest order mode within the cavity is

$$E_z = \cos\frac{\pi x}{w}\sinh\{pk(y+d)\}$$

where now

$$p = \sqrt{\left(\frac{\lambda}{2w}\right)^2 - \varepsilon'\mu'} \tag{45}$$

rom which it follows that

$$\eta = -iZ\frac{\mu'}{p}\tanh(pkd) \tag{46}$$

We note that for small w/λ and d comparable to or greater than w, $\eta \approx -iZ\,u'/p$ independent of the depth d.

If the cavity has no metal base as in Figure 9(b), the analogous expressions for η are

$$\eta = -iZ\frac{p}{\varepsilon'}\frac{\tan(pkd) + i\frac{\varepsilon'}{p}Z_1}{1 + i\frac{\varepsilon'}{p}Z_1\tan(pkd)} \tag{47}$$

for H-polarization and

$$\eta = -iZ \frac{\mu'}{p} \frac{\tanh(pkd) + i \frac{p}{\mu'} Z_1}{1 + i \frac{p}{\mu'} Z_1 \tanh(pkd)} \tag{48}$$

for E-polarization, where Z_1 is the relative impedance at the lower surface of the insert looking into the region $y < -d$. For a still more realistic (butted) geometry such as that shown in Figure 9(c), the impedance can be computed using a quasi-static code.

References

[1] M.I. Herman and J.L. Volakis, "High Frequency Scattering by a Resistive Strip and Extensions to Conductive and Impedance Strips," Radio Sci., vol. 22, no. 3, pp. 335-349, 1987.

[2] M.A. Ricoy and J.L. Volakis, "Integral Equations with Reduced Unknowns for the Simulation of Two-Dimensional Composite Structures," submitted to IEEE Trans. Antennas Propagat.

[3] T.B.A. Senior, "Some Extensions of Babinet's Principle in Electromagnetic Theory," IEEE Trans. Antennas Propagat., vol. AP-25, no. 3, pp. 717-720, 1977.

[4] _____, "Backscattering from Resistive Strips," IEEE Trans. Antennas Propagat., vol. AP-27, no. 6, pp. 808-813, 1979.

[5] _____, "A Critique of Certain Half-Plane Diffraction Analyses," Electromagnetics, vol. 7, pp. 81-90, 1987.

[6] N.I. Muskhelishvili, Singular Integral Equations. P. Nordhoff, Groningen, Holland, 1953; pp. 373 et seq.

[7] F.G. Tricomi, Integral Equations. Dover Publications, Inc., New York, N.Y., 1985.

[8] D.R. Wilton and C.M. Butler, "Effective Methods for Solving Integral and Integro-Differential Equations," Electromagnetics, vol. 1, pp. 289-308, 1981.

[9] J.J. Bowman, T.B.A. Senior and P.L.E. Uslenghi, Electromagnetic and Acoustic Scattering by Simple Shapes. Hemisphere Pub. Corp., New York, N.Y., 1987; pp. 189 and 209.

[10] M.A. Ricoy, S.M. Kilberg and J.L. Volakis, "Simple Integral Equations for Two-Dimensional Scattering With Further Reduction in Unknowns," submitted to Proc. IEE (London).

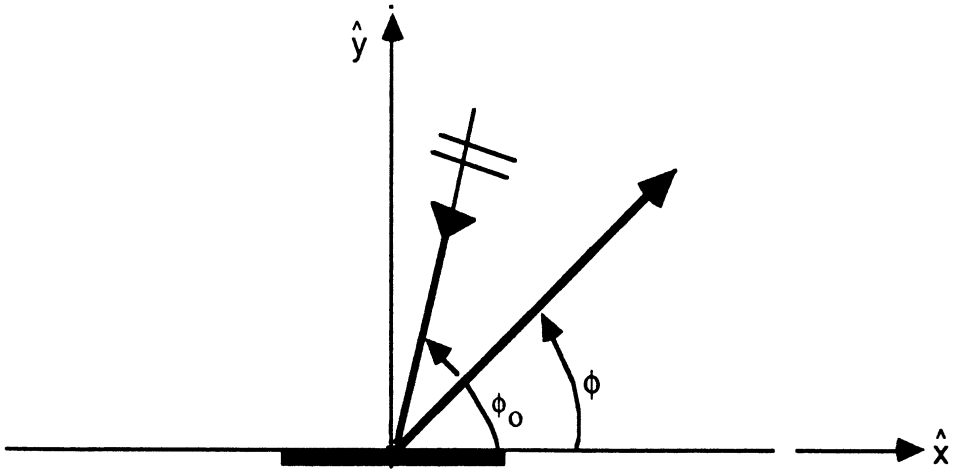

Fig. 1. Geometry of the resistive or impedance insert

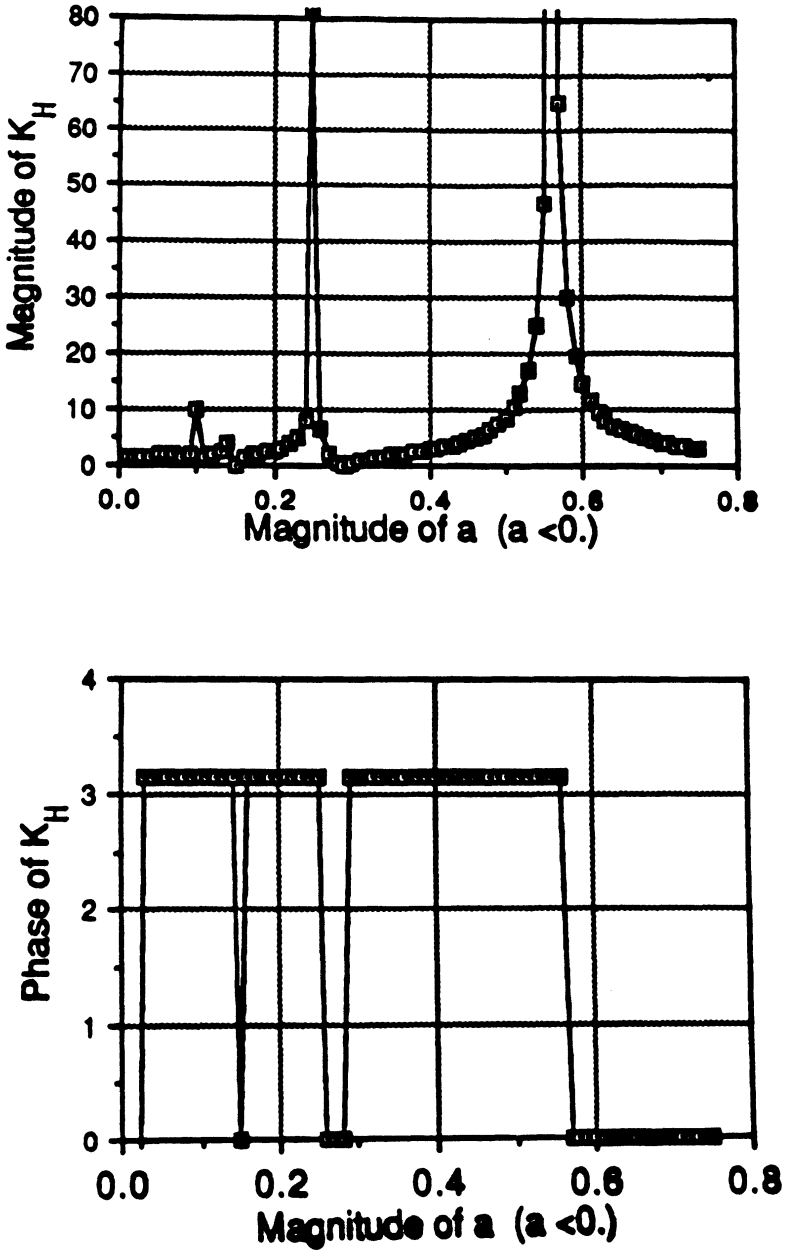

Fig. 2. Plot of the amplitude and phase of K_H (a) for a real and negative.

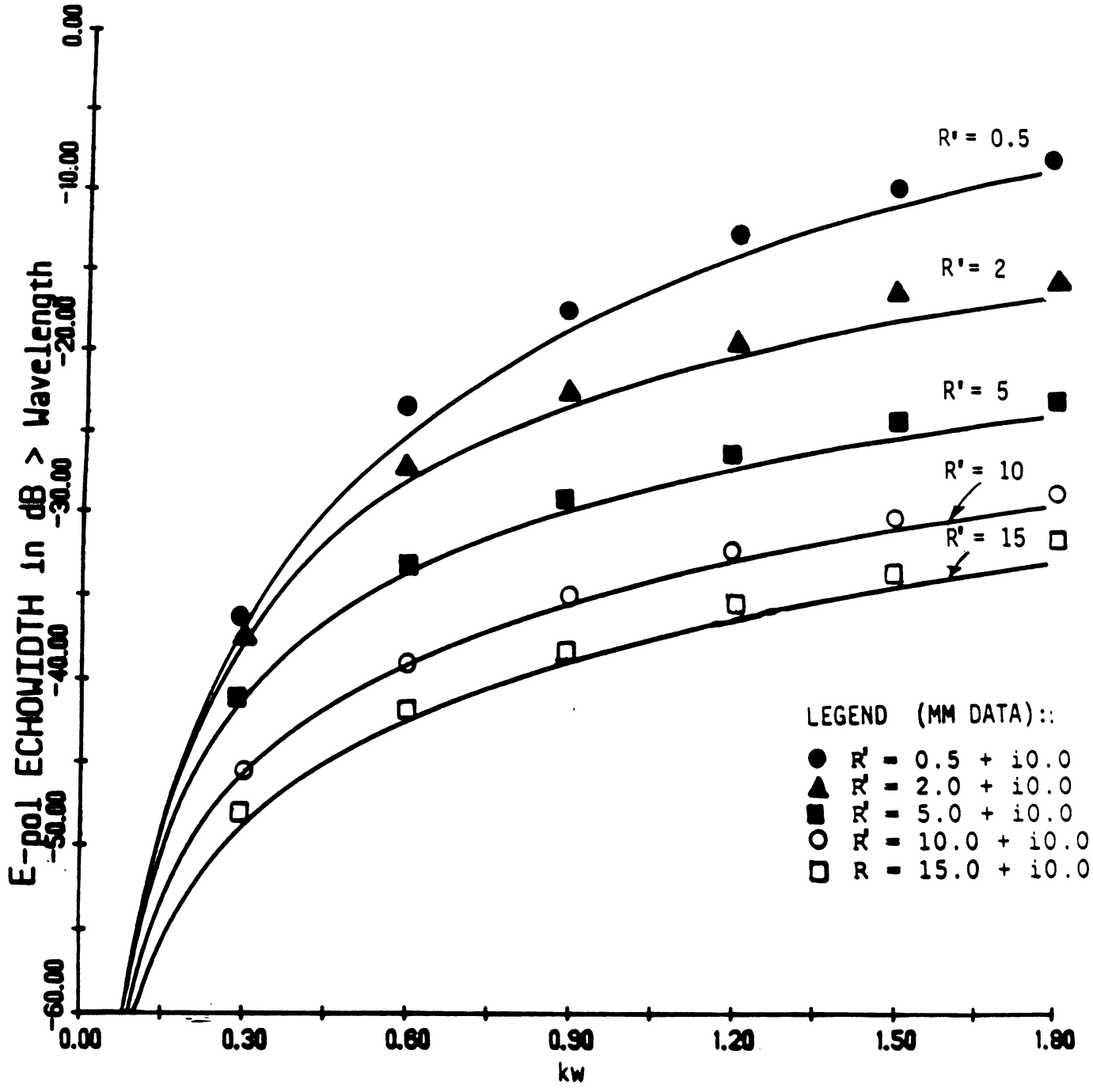

Fig. 3. Comparison of the backscatter echowidth, σ_E, as computed by (37) and the moment method [2] with $\phi = \phi_o = \pi/2$ for inserts having resistivities $R = Z^2/4R'$ where $R' = 0.5, 2.0, 5.0, 10$ and 15.

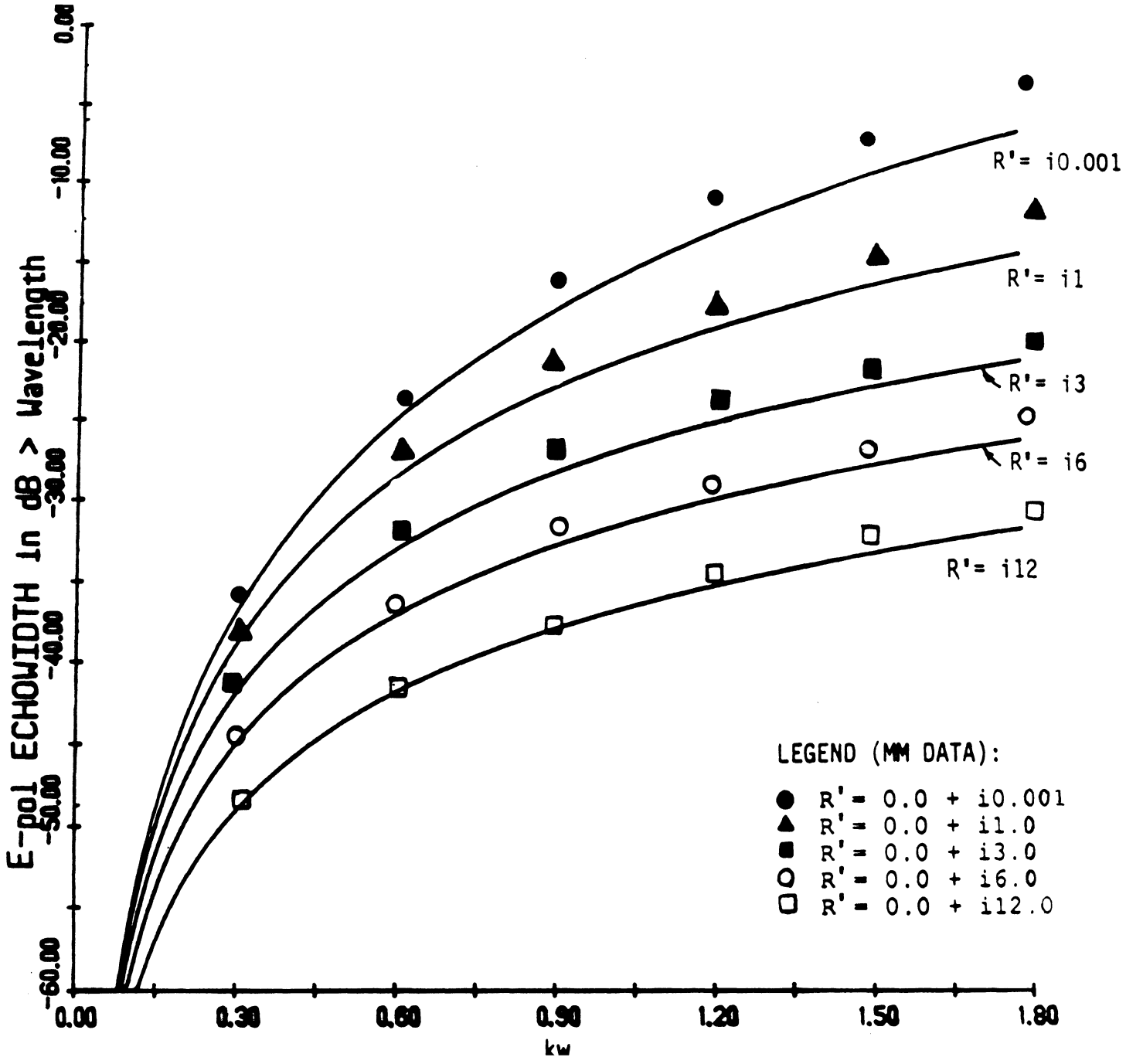

Fig. 4. Comparison of the backscatter echowidth, σ_E, as computed by (37) and the moment method [2] with $\phi = \phi_0 = \pi/2$ for inserts having resistivities $R = Z^2/4R'$ where $R' = i0.001$, i1.0, i3.0, i6.0 and i12.0.

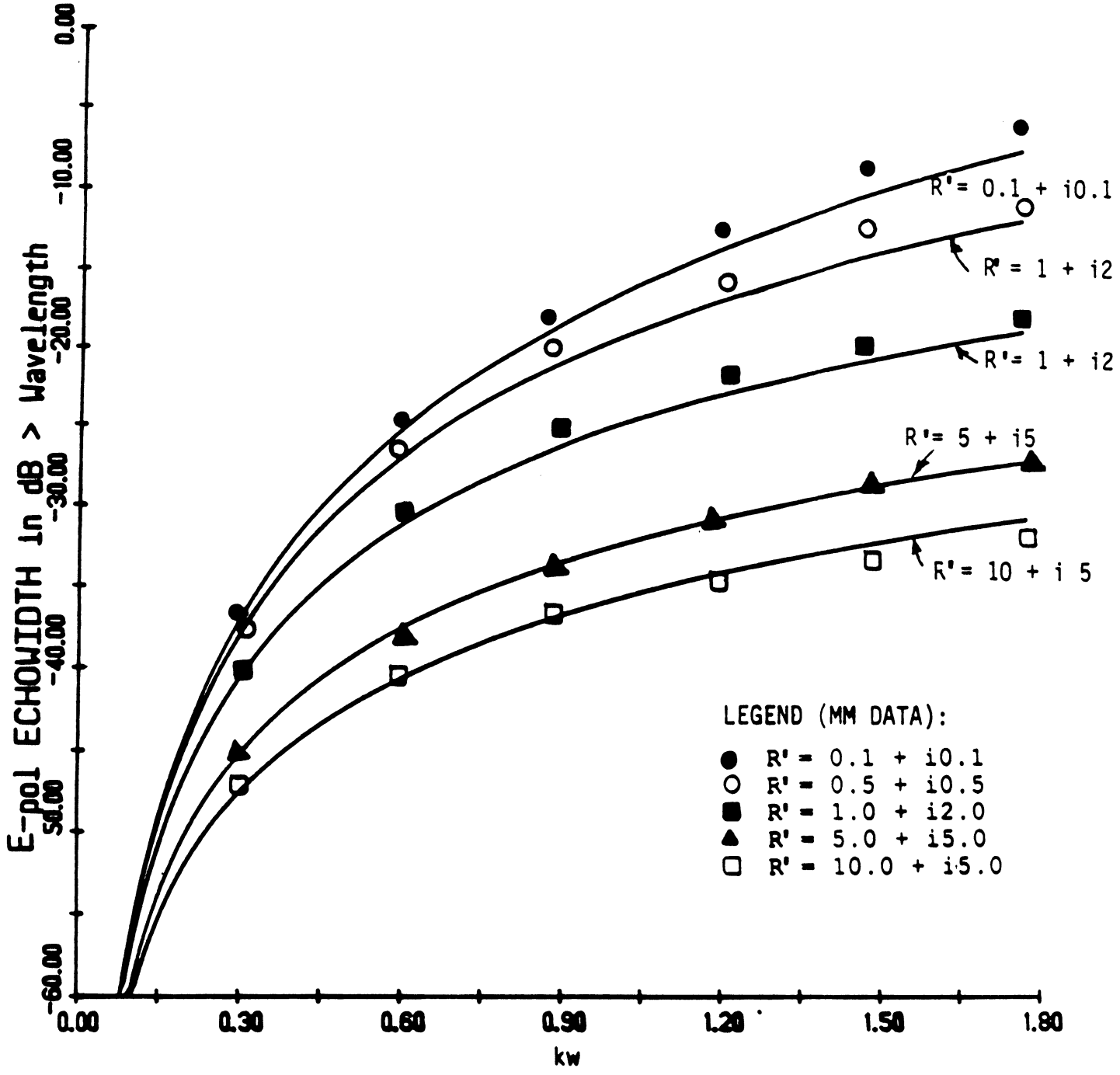

Fig. 5. Comparison of the backscatter echowidth, σ_E, as computed by (37) and the moment method [2] with $\phi = \phi_0 = \pi/2$ for inserts having resistivities $R = Z^2/4R'$ where $R' = 0.1 + i0.1$, $0.5 + i0.5$, $1.0 + i2.0$, $5.0 + i5.0$ and $10.0 + i15.0$.

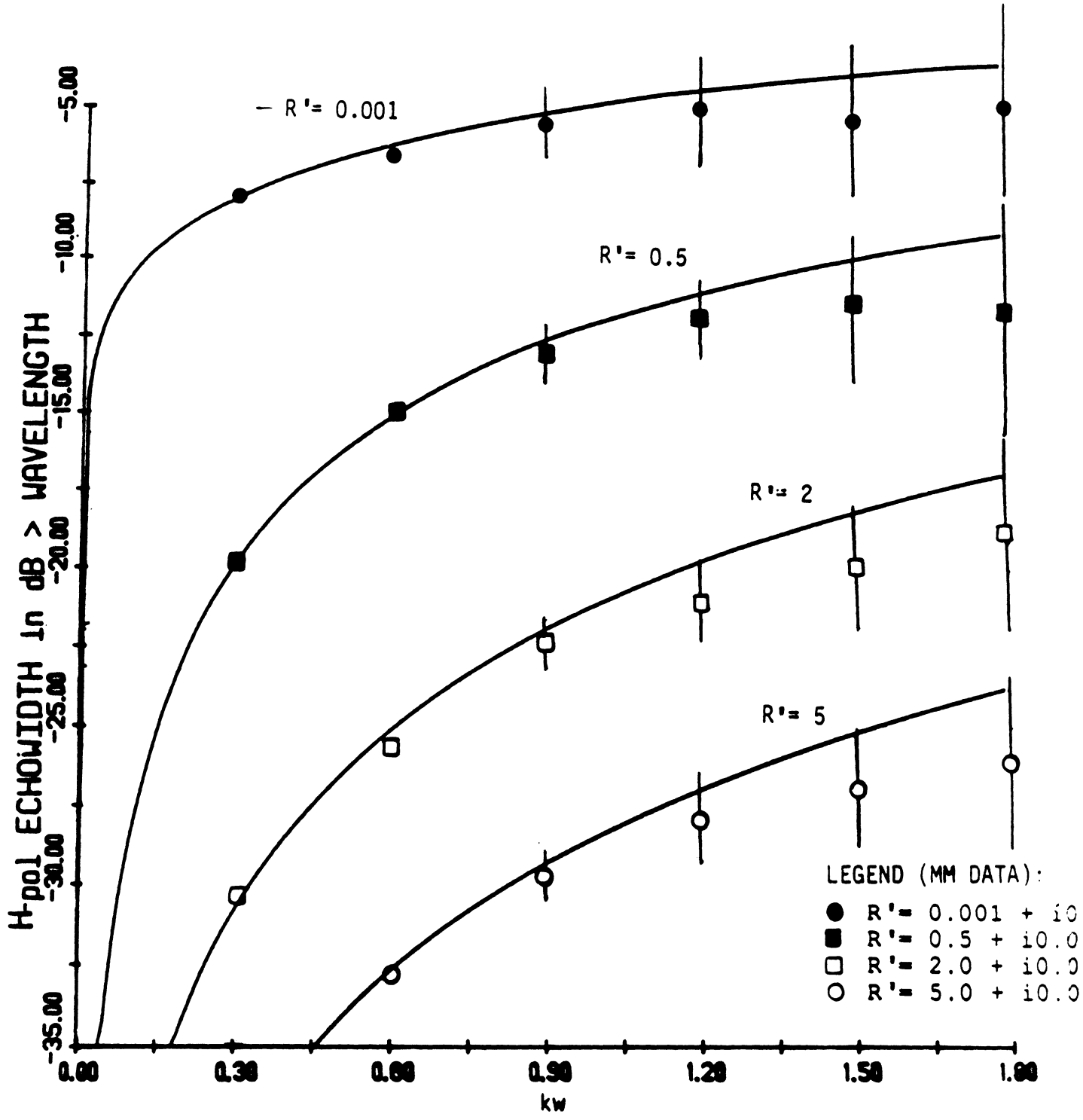

Fig. 6. Comparison of the backscatter echowidth, σ_H, as computed by (28) and the moment method [2] for inserts having resistivities $R = Z^2/4R'$ where $R' = .001, 0.5, 2.0$ and 5. The bar lengths correspond to the variation of σ_H in the range $0 < \phi < \pi/2$.

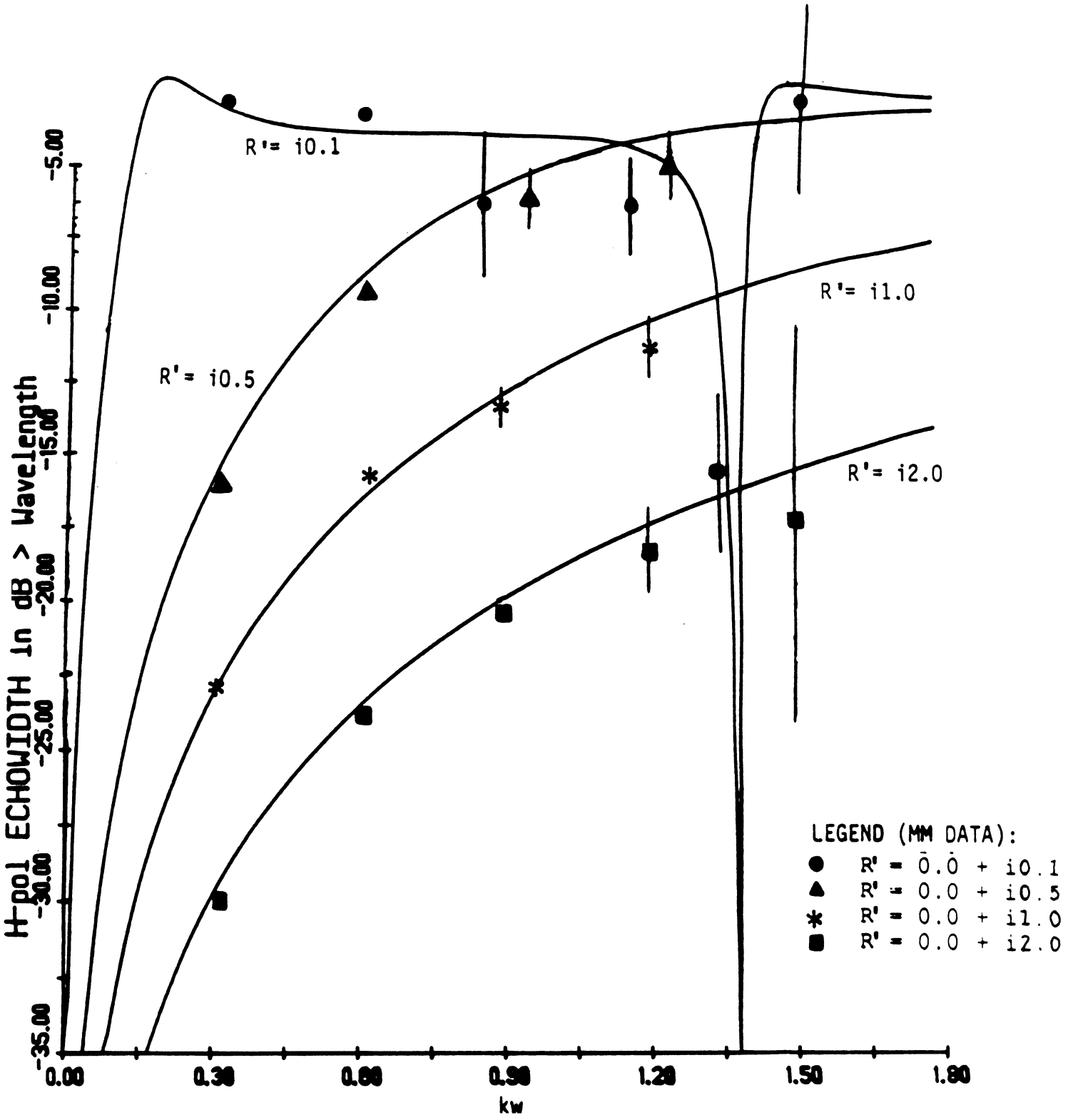

Fig. 7. Comparison of the backscatter echowidth, σ_H, as computed by (28) and the moment method [2] for inserts having resistivities $R = Z^2/4R'$ where R = i0.1, i0.5, i1.0 and i2.0. The bar lengths correspond to the variation of σ_H in the range $0 < \phi < \pi/2$.

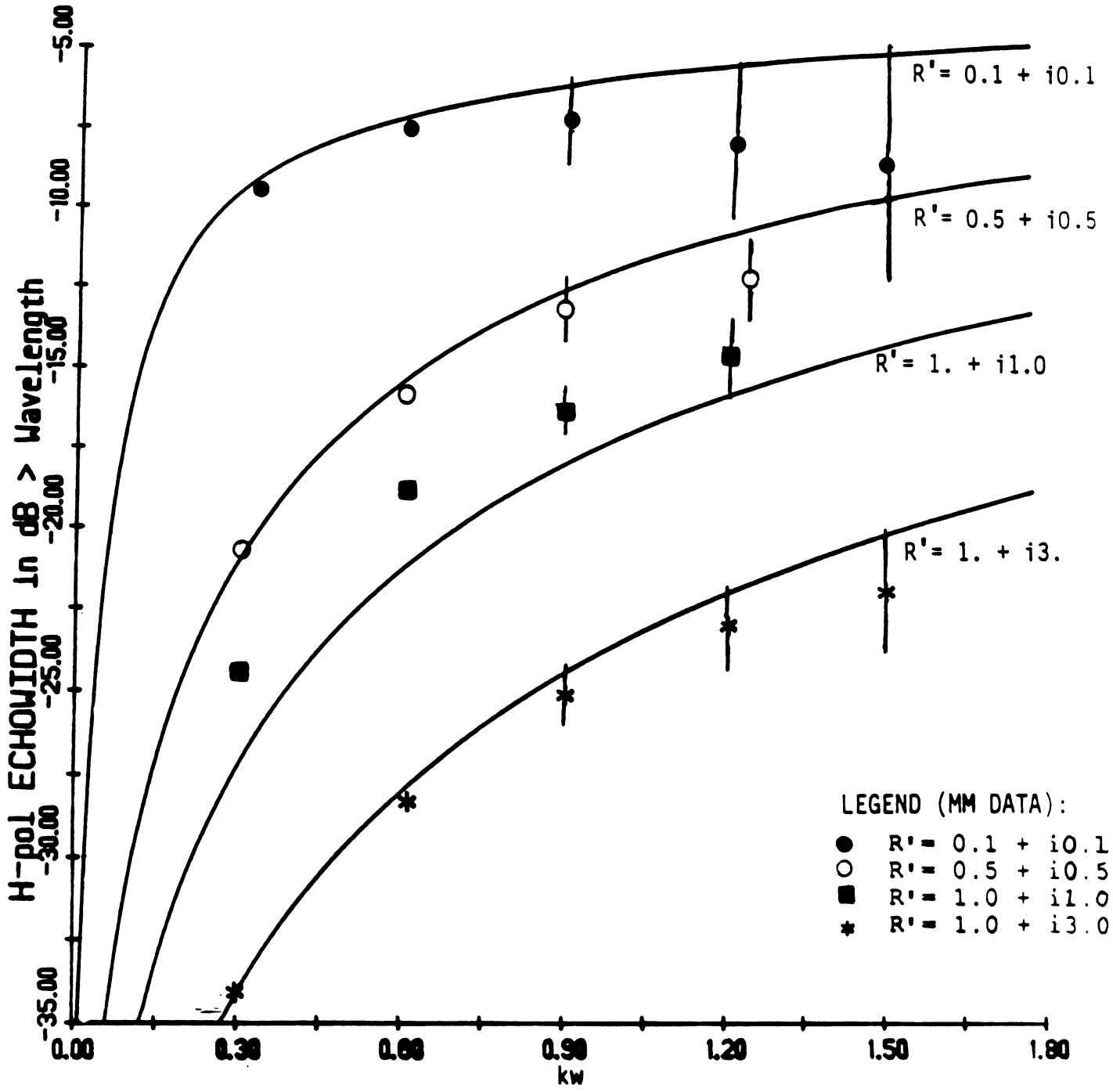

Fig. 8. Comparison of the backscatter echowidth, σ_H, as computed by (28) and the moment method [2] for inserts having resistivities $R = Z^2/4R'$ where$R = 0.1 + i0.1$, $0.5 + i0.5$, $1.0 + i1.0$ and $1.0 + i3.0$. The bar lengths correspond to the variation of σ_H in the range $0 < \phi < \pi/2$.

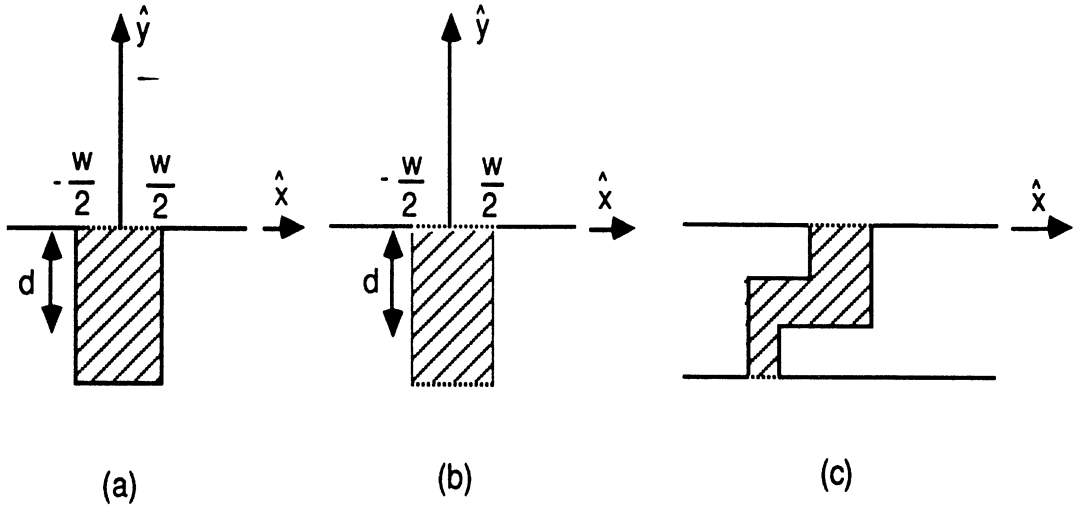

Fig. 9. Illustration of some gap and crack geometries of practical interest.

Appendix A Determination of the Gap Impedance (Mr. S.M. Kilberg)

For gaps other than the closed or open rectangular cavity-backed slots shown in Figures 9(a) and (b), no quasi-static analytical technique has yet been found to compute the impedance, though we still believe that this should be possible for a few other geometries at least. We are continuing to pursue this and are also developing a numerical approach valid for a wide range of geometries that makes use of the electrically small dimensions of the gap. Meanwhile, to verify the analytical expressions for the single gap geometries given in Section 4, and to provide some data for more complicated geometries, we have computed the gap impedance using an existing dynamic moment method code [10].

The code utilizes a computationally efficient and simple set of volume/surface integral equations to model two-dimensional scatterers of arbitrary shape and composition. Based on the known equivalence between electric and magnetic currents, the scattered field is expressed in terms of a single component of an equivalent current at each sampling point. This reduces the demands on computer resources (CPU time and memory allocation) and provides an efficient method for computing the currents and, hence, near and far field scattering for electrically large bodies. Within the program the matrix elements are computed using pulse basis functions and point matching. For the diagonal (self cell) and near diagonal elements of the matrix, the integrations are performed analytically to minimize the errors inherent in dealing with electrically small features. Having found the current, the components of the total electric and magnetic fields are computed at intervals of 0.01λ across the aperture of the slot. The local impedances are then determined and averaged over the slot to give the effective impedance looking in.

The gap geometries of interest are shown in Fig. A-1, and the gaps -- open or closed (i.e. shorted) -- may be either air or dielectric filled. Since the computer program cannot handle the infinite, perfectly-conducting ground plane associated with these, all of the geometries were evaluated in the presence of the cylindrical ground planes shown in Fig. A-2. For each polarization, the ground plane was chosen to

minimize extraneous edge and surface wave effects while retaining an adequate simulation of the gap geometry.

A.1 Results for $\bar{E}$-Polarization

The computer program was first used to check the validity of (46) and (48) in the simple case of an air-filled rectangular gap. For both the open and shorted cavities the agreement is excellent for $w \leq 0.2\lambda$ and adequate for $w \leq 0.3\lambda$ for all values of the gap depth d that were examined. The comparison for the shorted cavities is given in Fig. A-3. Though the spatial distributions of the impedance values over the slot showed some dependence on the angle of incidence ϕ_0, the averages were relatively independent of ϕ_0 for ϕ_0 up to about 40 degrees, and the variation decreased with decreasing w/λ. The data also shows that for $d \geq$ max. $(w, 0.2\lambda)$ the impedance is almost independent of d, and this is expected since a narrow gap can support only an evanescent mode. The analogous expressions for the impedances of dielectric-filled gaps were also confirmed numerically.

Results for slanted, open air-filled cavities (see Fig. A-1(b)) are shown in Figs. A-4, 5 and 6, and compared with the analytical expression (48) with $Z_1 = Z$ for a rectangular (i.e. unslanted) cavity. The agreement is reasonably good for $w \leq 0.2\lambda$ but is significantly improved if the gap width used in (48) is measured perpendicular to the cavity walls, i.e. if $w \cos \alpha$ is used in place of w. The resulting expression for p is

$$p = \sqrt{\left(\frac{\lambda}{2w\cos\alpha}\right)^2 - \varepsilon'\mu'} \quad , \tag{A.1}$$

and with p defined in this manner, the impedances based on (48) are indicated by the dashed lines in Fig. A-6.

More complicated geometries are shown in Figs. A-7 and 8, and because of the large number of dimensions which are now involved, we have chosen to tabulate the results for a small selection. These confirm the validity of (46) and (48) with w and d identified as the width and depth of the initial rectangular portion. Analogous results

for a still more realistic geometry typical of the junction betwen two component structures are presented in Figs. A-9 and 10.

In summary, the fact that for E-polarization a narrow gap can support only an evanescent mode implies that for an initial cavity whose depth exceeds (about) 0.2λ the impedance is independent of the substructure, thereby allowing us to use the analytical expression (46) or (48) as appropriate. If the initial cavity is slanted, p should be defined as in (A.1). For (initial) gap widths $w \leq 0.3\lambda$, the accuracy of the resulting impedance is better than 10 percent.

A.2 Results for H-Polarization

The numerical computation of the impedance is a much more difficult task for H-polarization, and though the cylindrical ground plane illustrated in Fig. A-1 reduces the edge effects associated with a terminated ground plane, it is not a perfect model of an infinite ground plane. Moreover, it does not enable us to model an open slot, and to test the validity of (47), the computations were carried out with an impenetrable plug of known relative impedance Z_1 inserted in the cavity. For an actual air-filled gap, $Z_1 \neq 1$ and depends on the properties of the region beneath.

For an open air-filled rectangular gap simulated by taking $Z_1 = 1$, (47) predicts $\eta = Z$ independent of w and d, and this is compared with the numerical results in Fig. A-11. The agreement is good considering the difficulty in enforcing the condition $Z_1 = 1$ at the plug. The analogous results for the shorted cavity are shown in Fig. A-12. The agreement with (44) is excellent and because the cavity now supports a propagating mode, there is a strong dependence on depth.

Since the dominant mode is a propagating one, the simple formulas (44) and (47) become increasingly inaccurate as the cavity departs from rectangular. Data for shorted air-filled slanted cavities of widths 0.1λ, 0.2λ and 0.3λ are shown in Figs. A-13, 14 and 15 respectively for three different slant angles and compared with the theoretical predictions for $\alpha = 0$. The errors increase with increasing α and there is no obvious redefiniton of w and/or d that makes (44) applicable. We note in passing that

the larger discrepancies for $w = 0.1\lambda$ vis-a-vis those for the larger gap widths are probably due to numerical errors in the dynamic code.

As a final test, the impedance presented by the more realistic shorted cavity in Fig. A-16 was computed. As the tabulated data shows, (44) is no longer applicable, and this is hardly surprising in view of the propagating nature of the cavity field. In contrast to the situation with E-polarization, the substructure of the gap has a dominating effect for H-polarization, and must be taken into account in computing the impedance. We are continuing to seek methods which will enable us to do this in a simple manner.

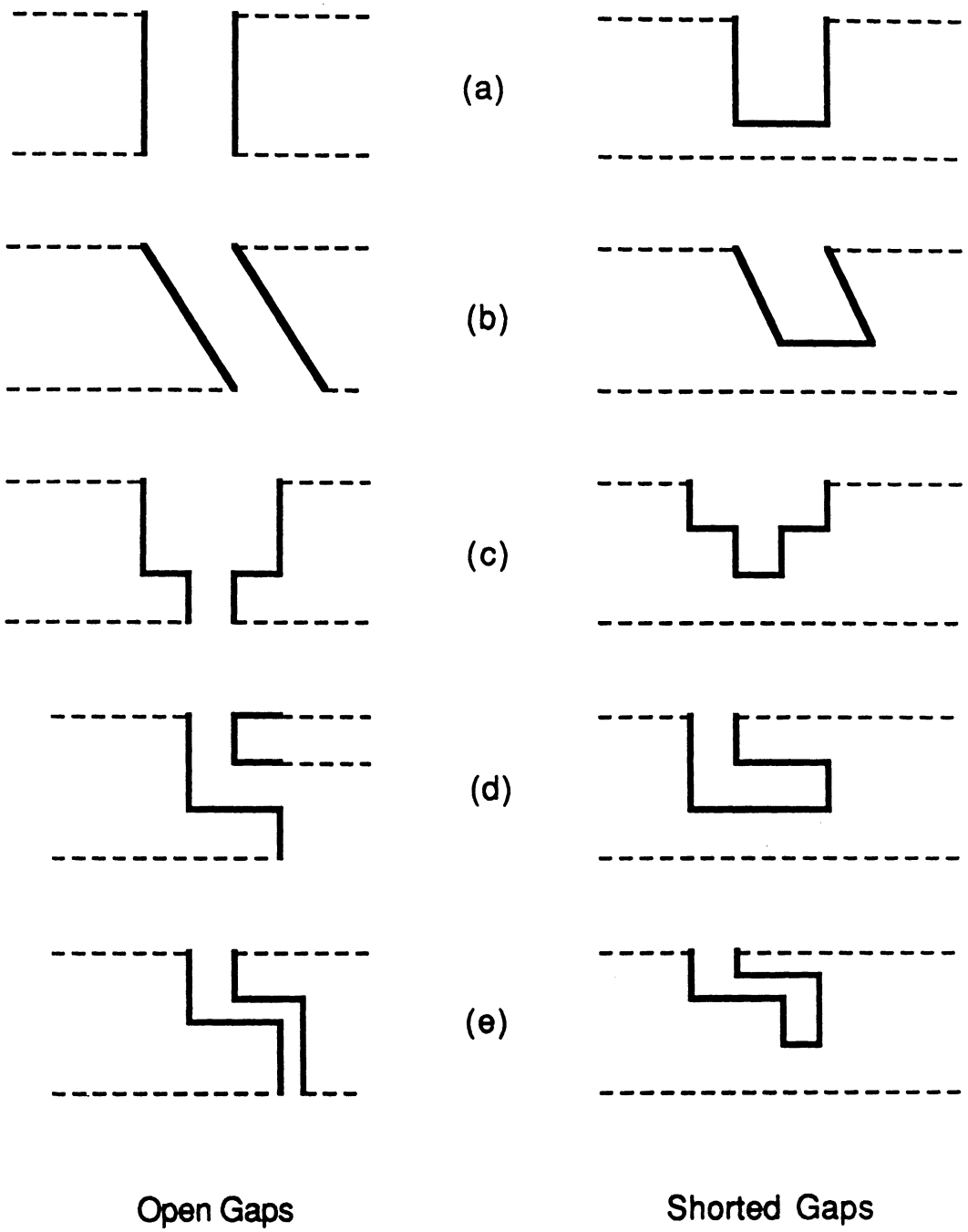

Fig. A-1: Gap geometries

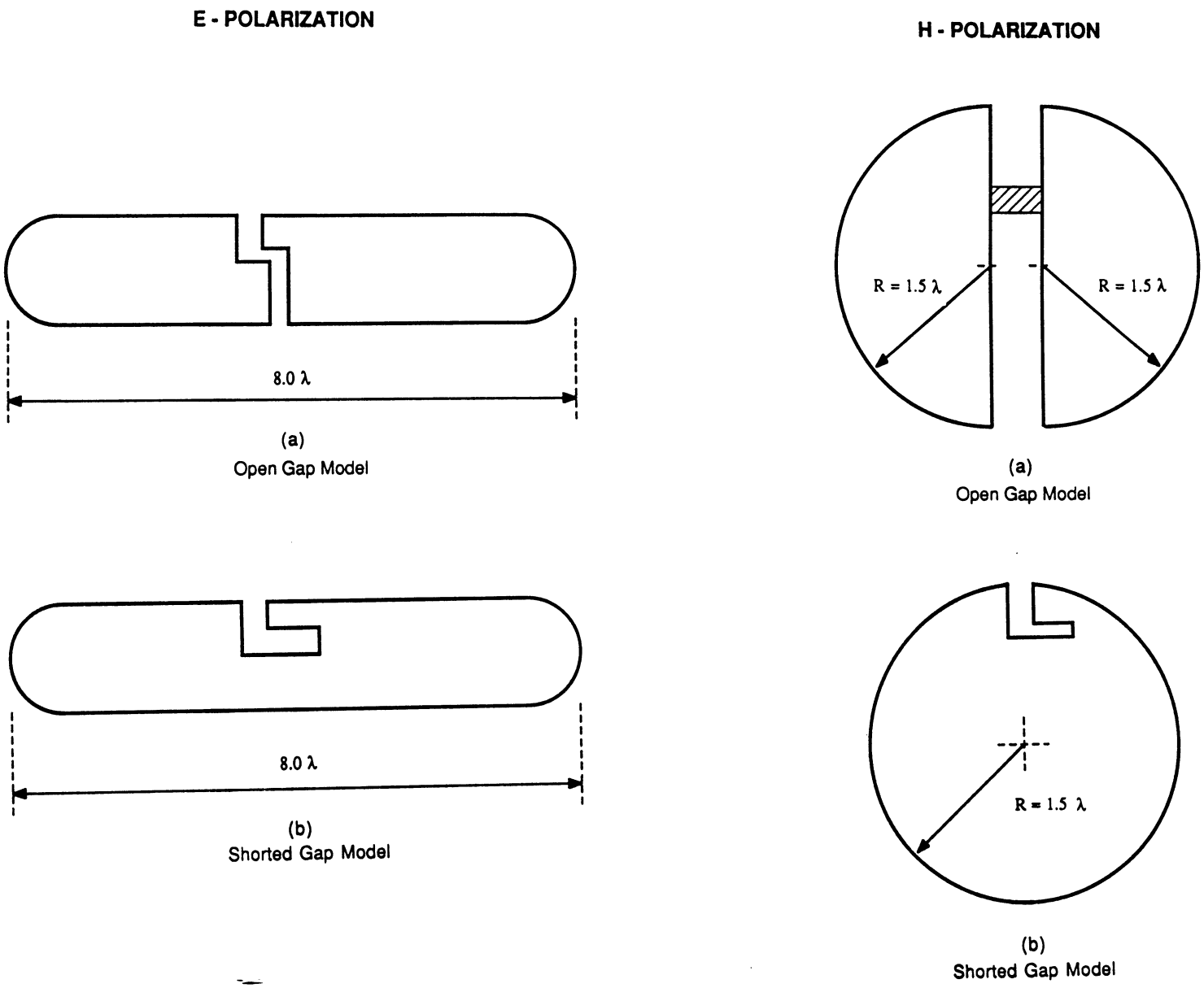

Fig. A-2: Ground plane configurations

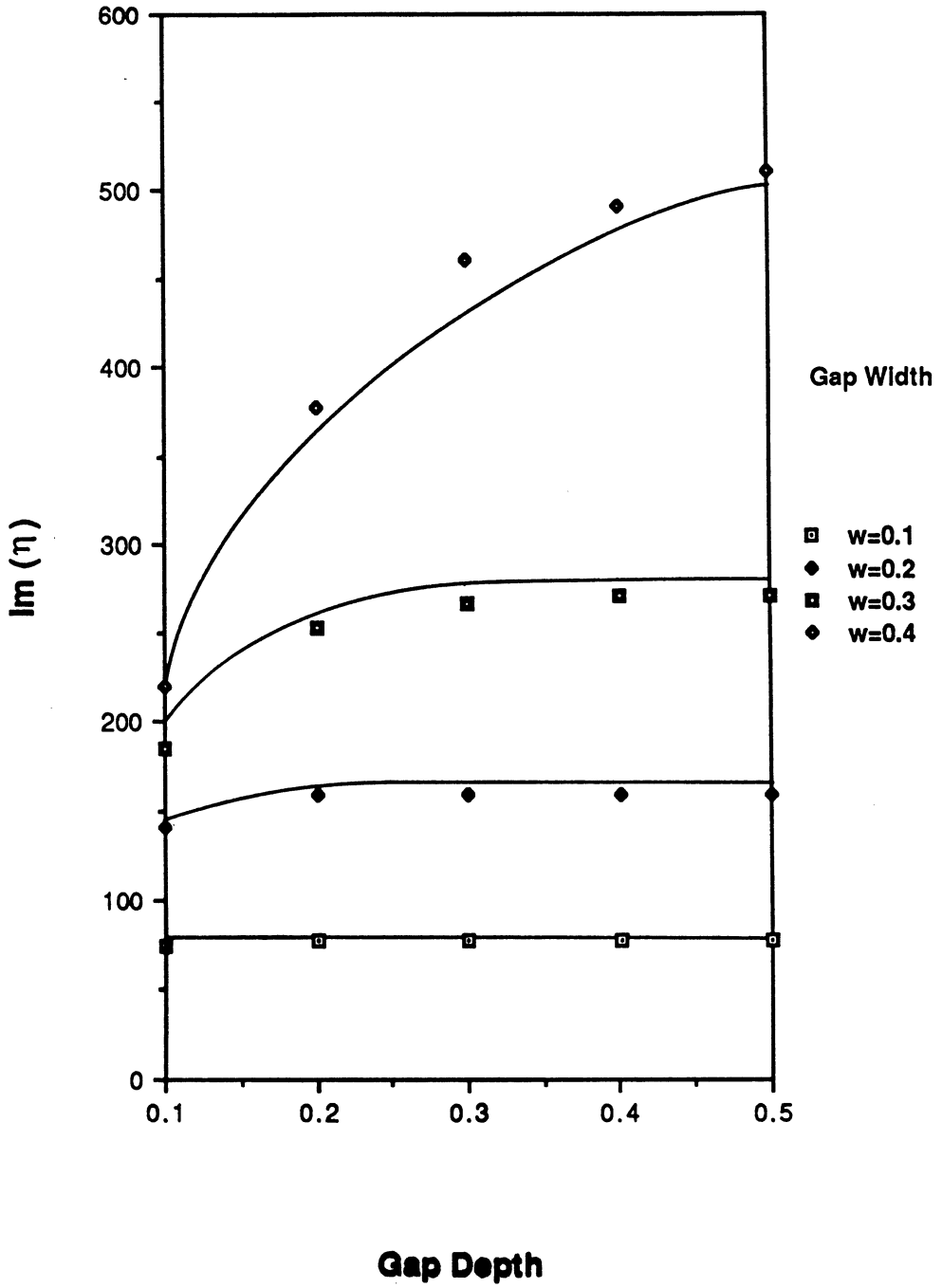

Fig. A-3: Shorted rectangular cavity, E-polarization. In this and all subsequent figures, the solid lines were derived from the analytical expressions, and the points were computed numerically. Dimensions are in wavelengths.

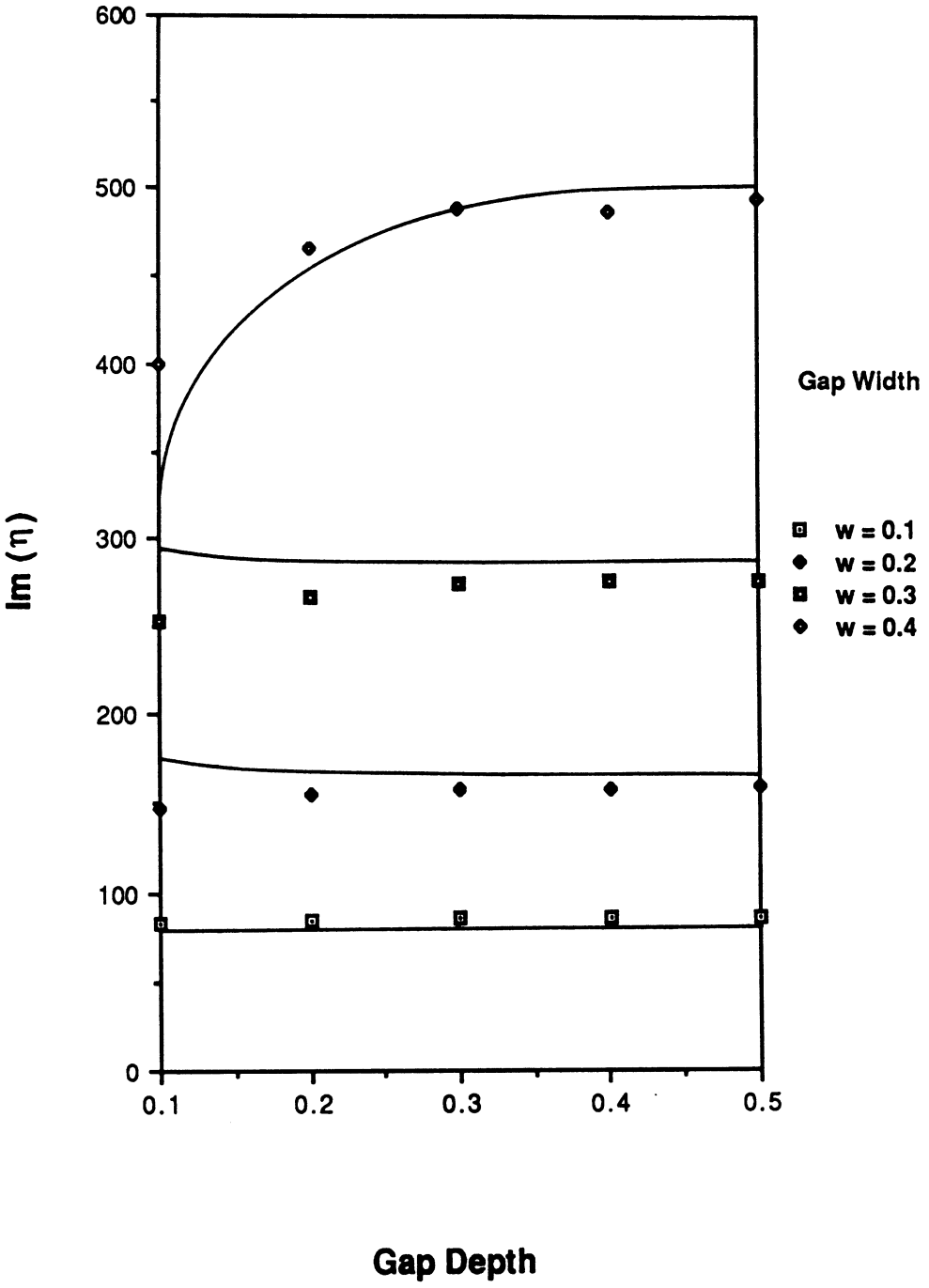

Fig. A-4: Open slanted cavity for E-polarization: slant angle α = 10 degrees

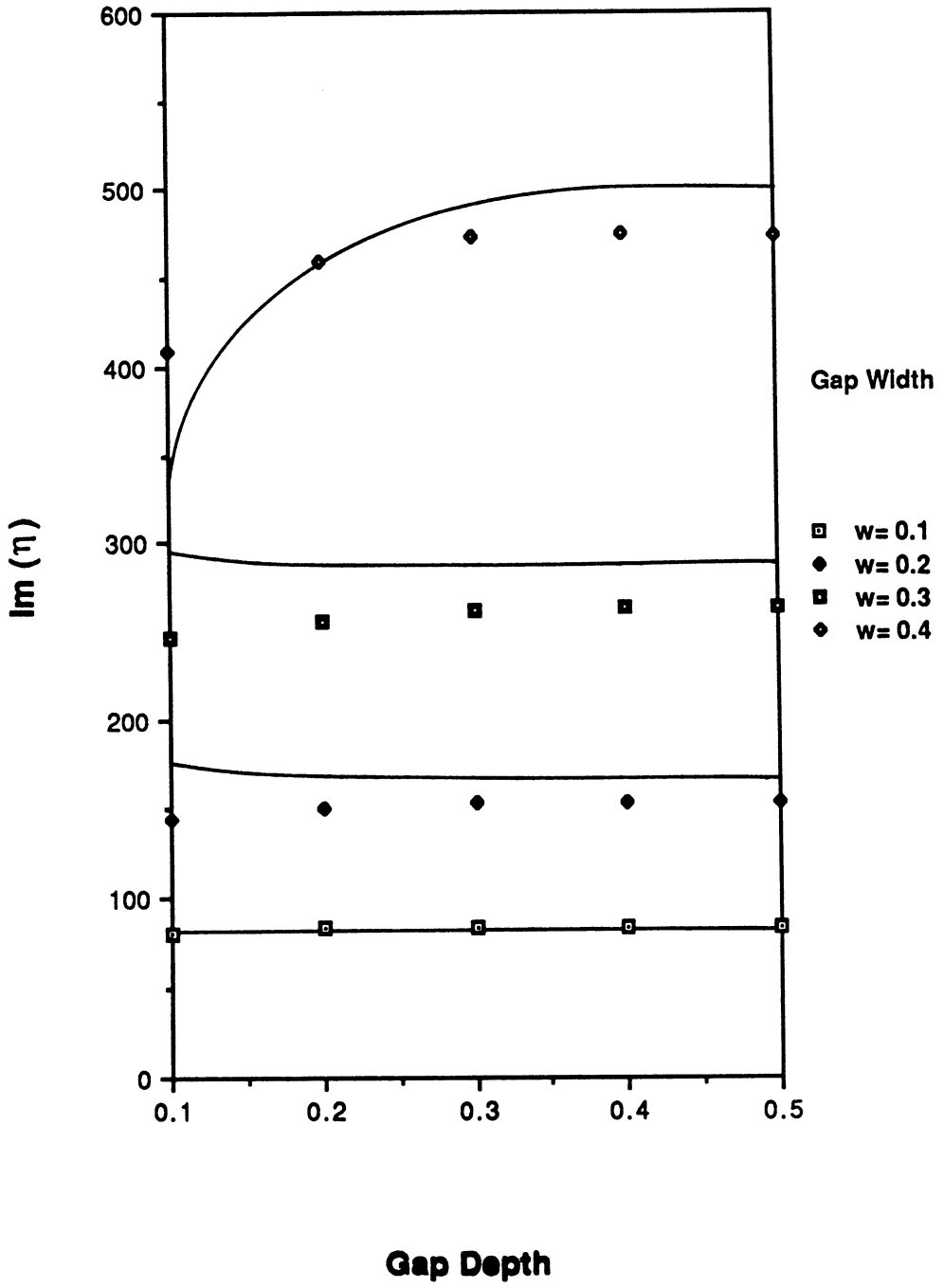

Fig. A-5: Open slanted cavity for E-polarization: slant angle α = 20 degrees

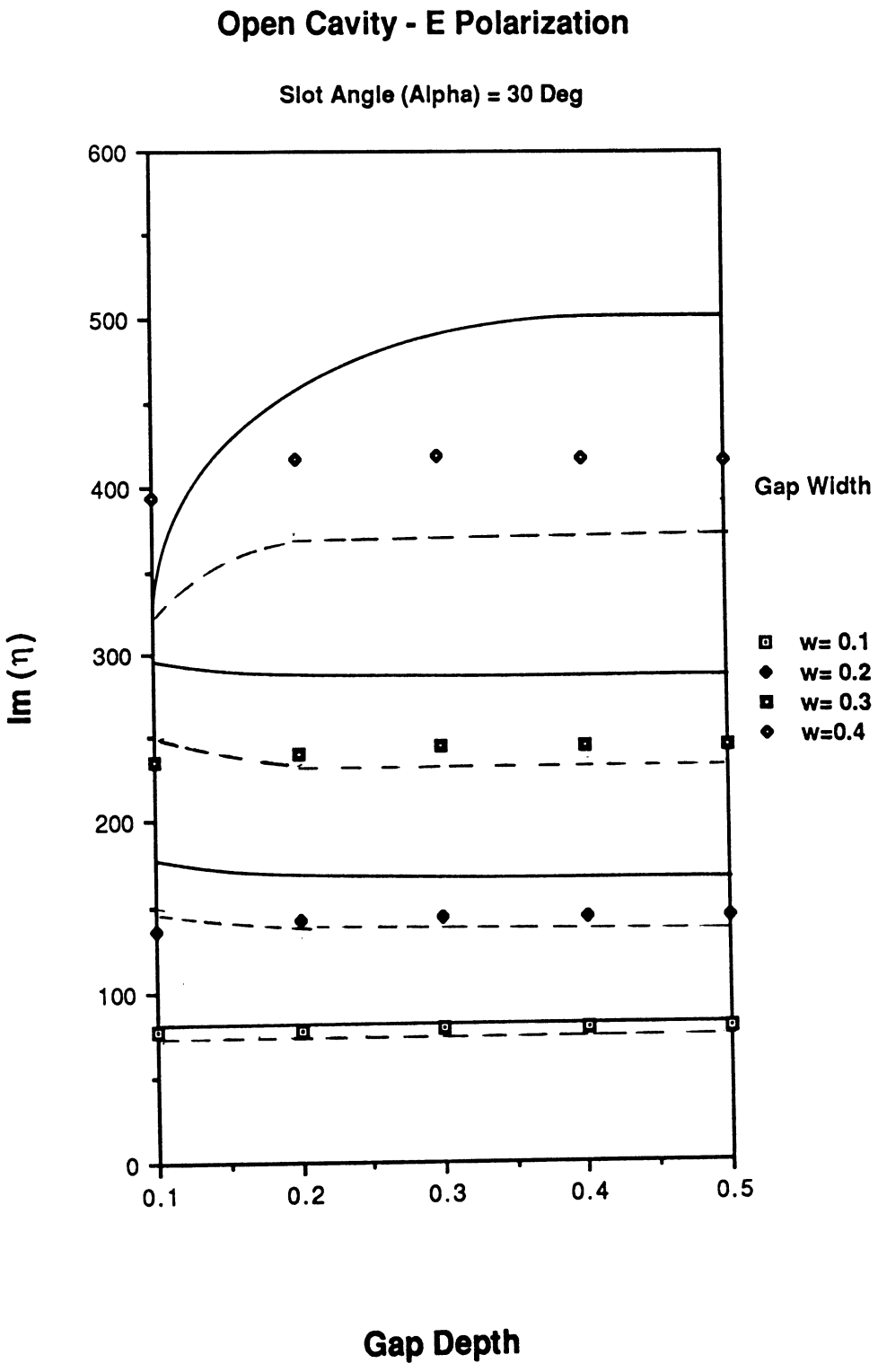

Fig. A-6: Open slanted cavity for E-polarization: slant angle α = 30 degrees.

Shorted Cavity - E Polarization

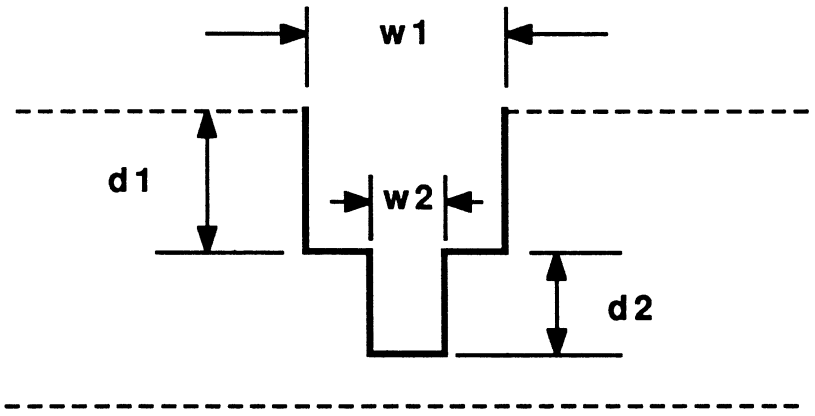

w1	d1	w2	d2	(46)	Num
0.3	0.2	0.1	0.2	-i264	-i266
0.3	0.2	0.1	0.1	-i264	-i270
0.2	0.2	0.1	0.2	-i165	-i169
0.2	0.2	0.1	0.2	-i165	-i170

Fig. A-7: Results for a shorted cavity, E-polarization

_Open Cavity - E Polarization

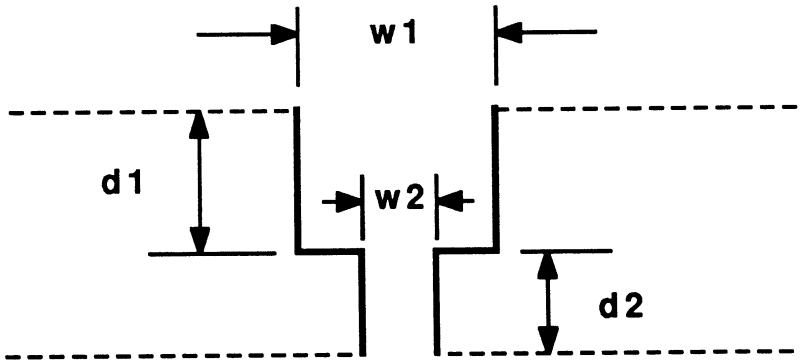

w1	d1	w2	d2	(48)	Num
0.3	0.2	0.1	0.2	-i288	-i266
0.3	0.2	0.1	0.1	-i288	-i270
0.2	0.2	0.1	0.2	-i165	-i169
0.2	0.2	0.1	0.2	-i165	-i170

Fig. A-8: Results for an open cavity, E-polarization

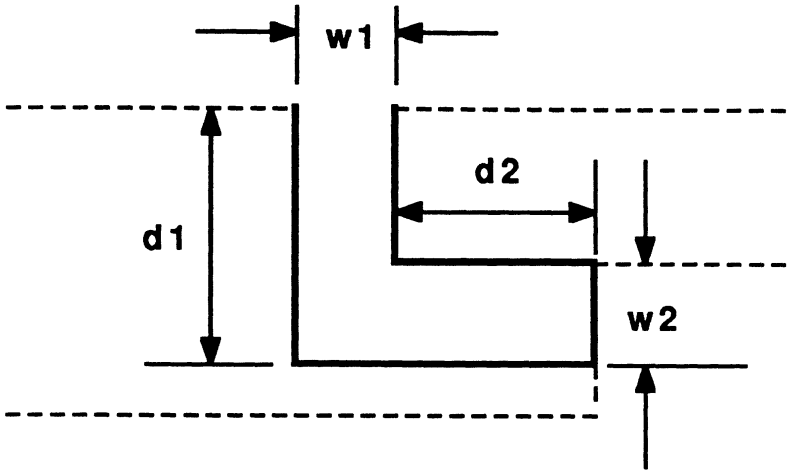

w1	d1	w2	d2	(46)	Num
0.3	0.2	0.1	0.5	-i264	-i271
0.3	0.2	0.1	0.2	-i264	-i272
0.3	0.3	0.2	0.2	-i264	-i270
0.2	0.2	0.1	0.5	-i164	-i165
0.2	0.3	0.1	0.2	-i164	-i168
0.2	0.3	0.1	0.2	-i164	-i168

Fig. A-9: Results for a shorted cavity, E-polarization

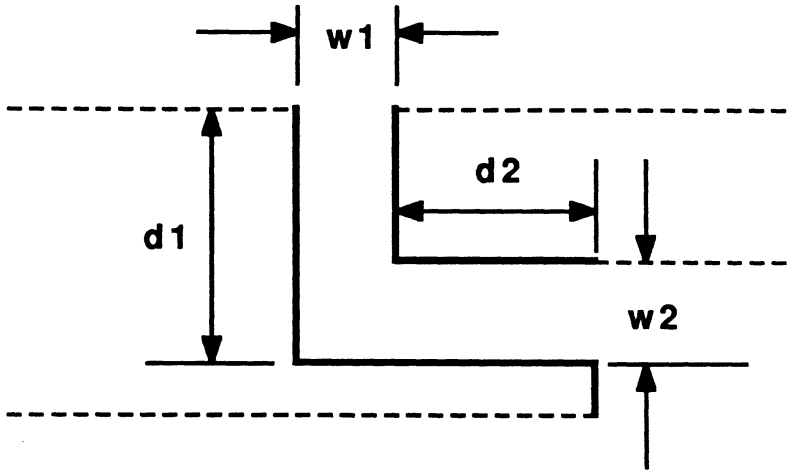

w1	d1	w2	d2	(48)	Num
0.3	0.2	0.1	0.5	-i288	-i271
0.3	0.2	0.1	0.2	-i288	-i275
0.3	0.3	0.2	0.2	-i284	-i274
0.2	0.2	0.1	0.5	-i165	-i170
0.2	0.3	0.1	0.2	-i165	-i172
0.2	0.3	0.1	0.2	-i165	-i172

Fig. A-10: Results for an open cavity, E-polarization

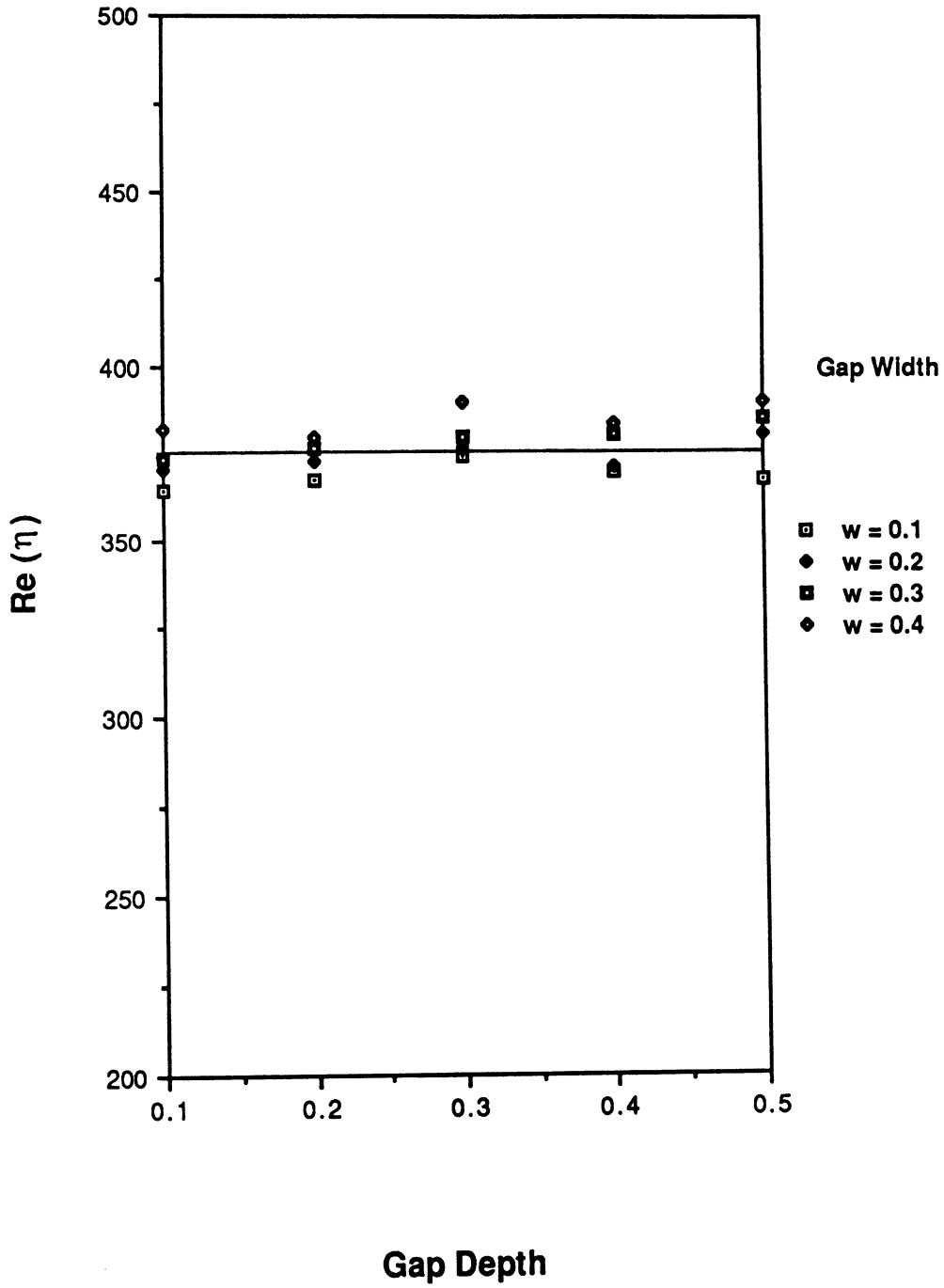

Fig. A-11: Open rectangular cavity, H-polarization with $Z_1 = 1$.

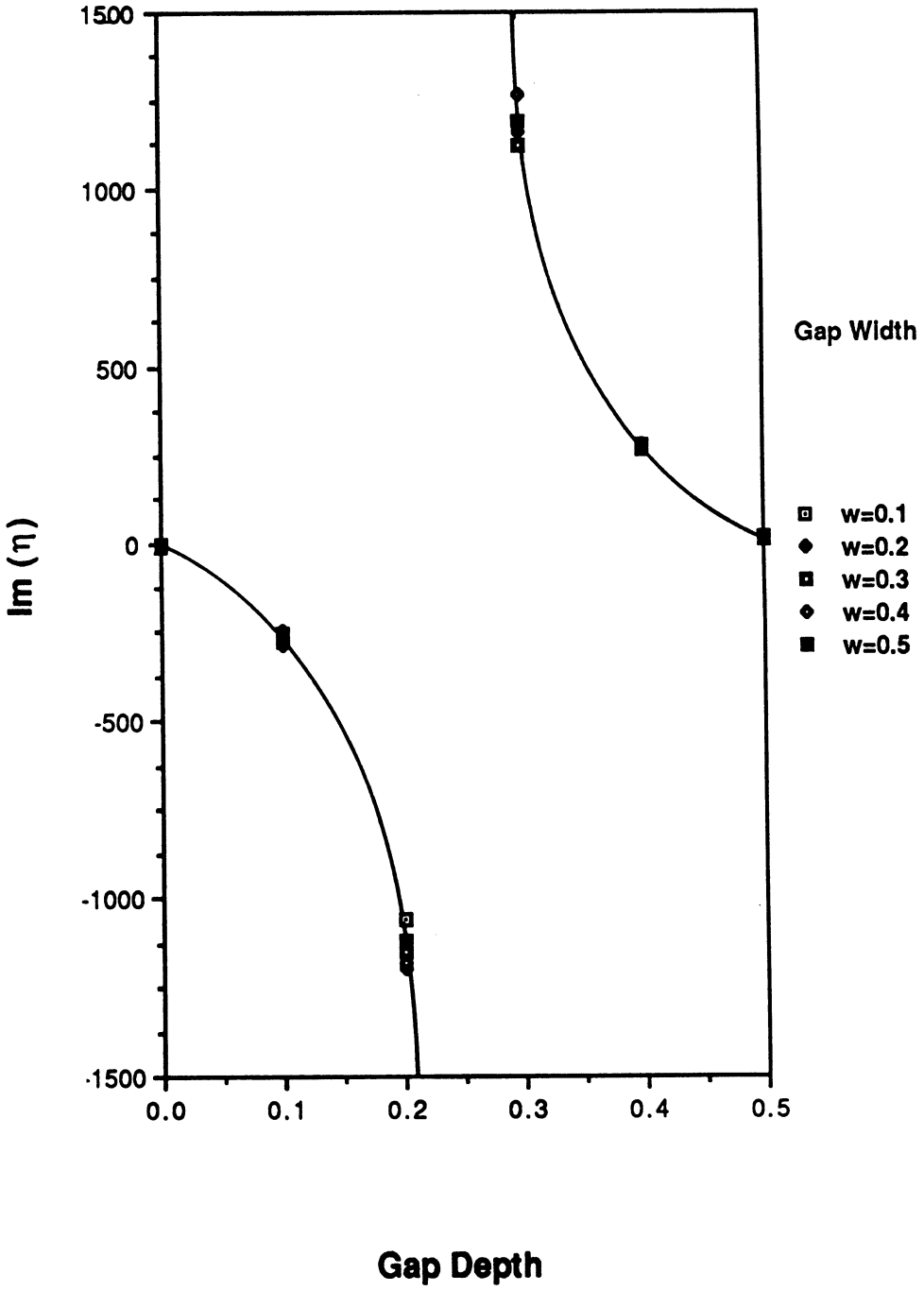

Fig. A-12: Shorted rectangular cavity, H-polarization

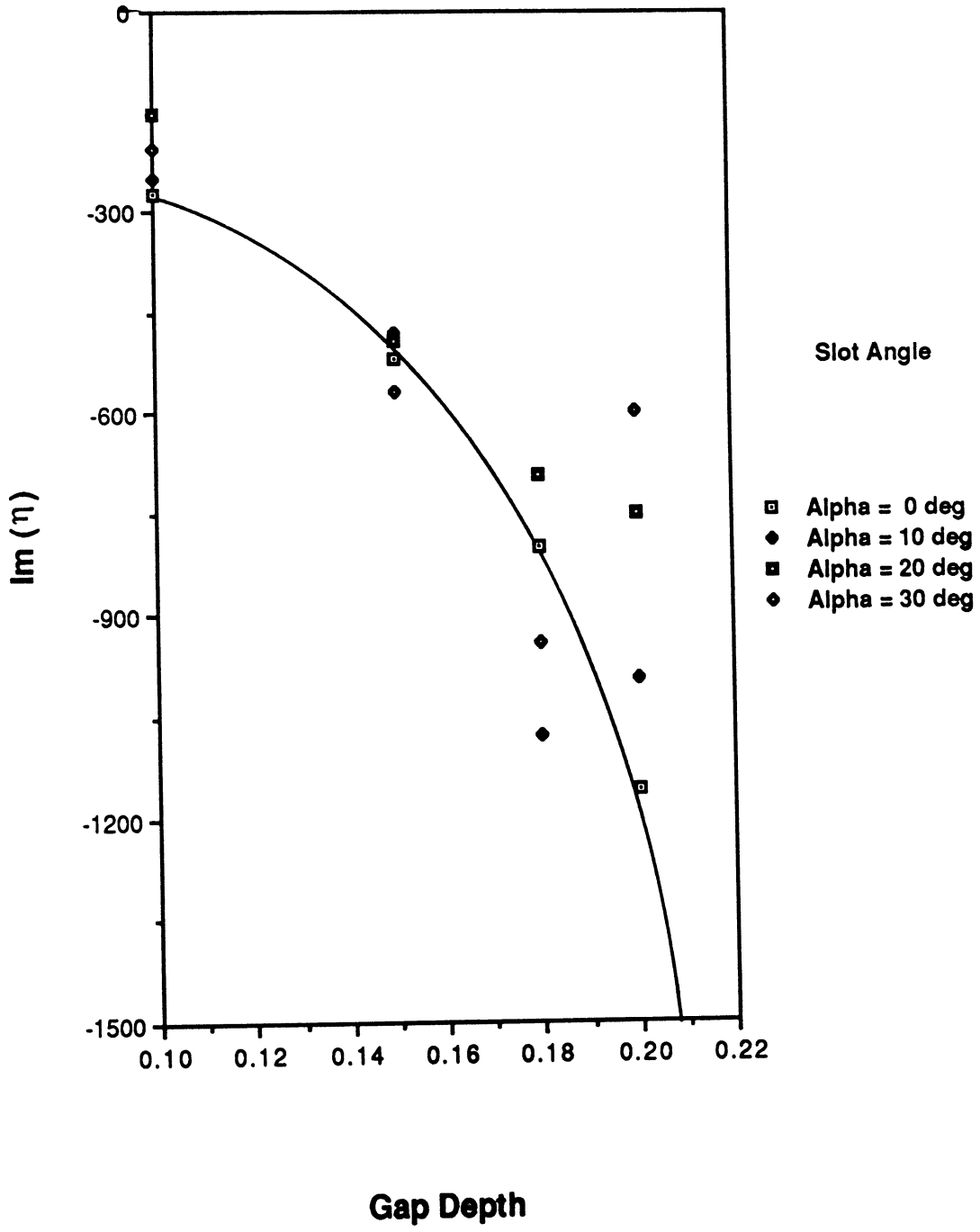

Fig. A-13: Shorted slanted cavities for w = 0.1λ, H-polarization

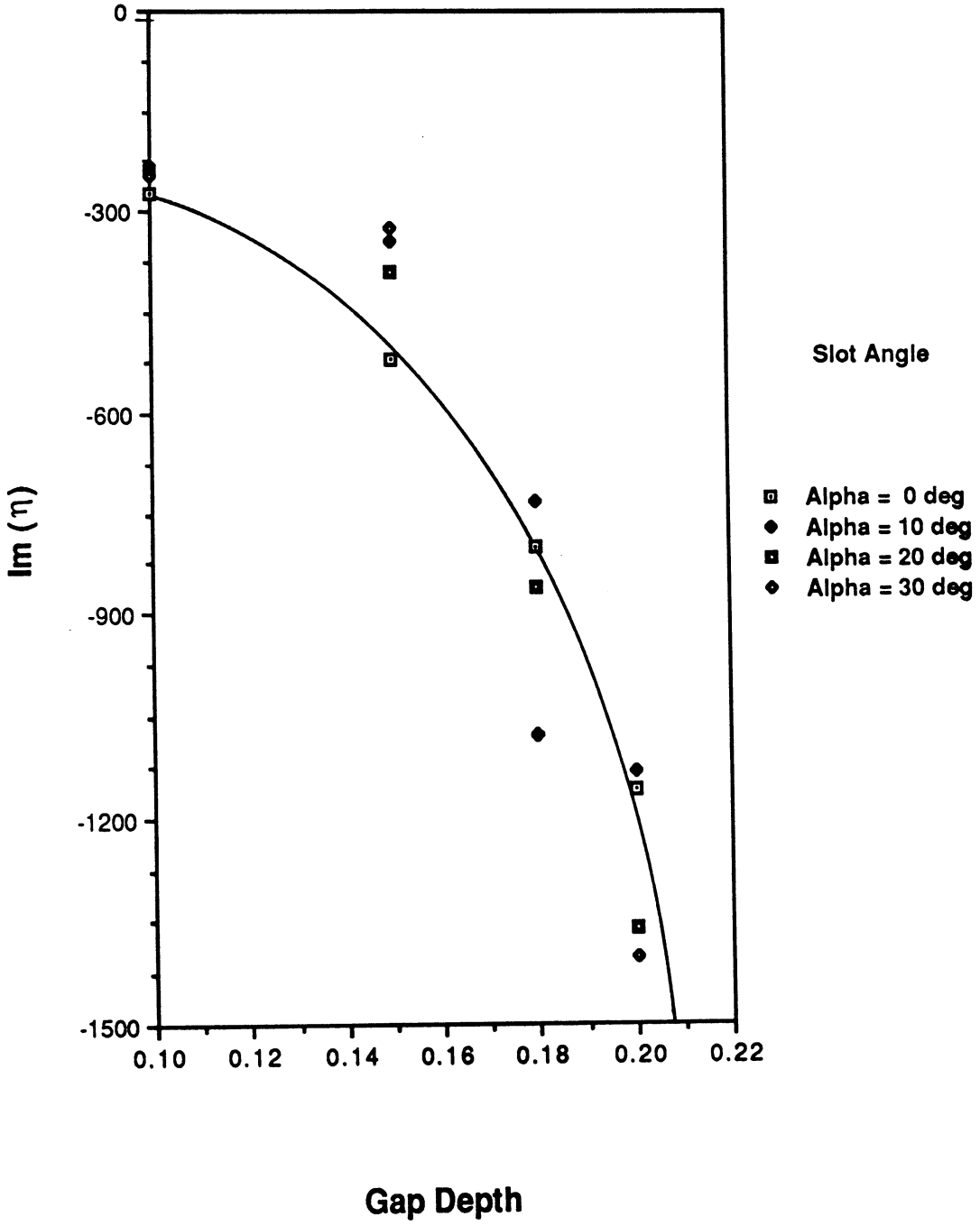

Fig. A-14: Shorted slanted cavities for w = 0.2λ, H-polarization

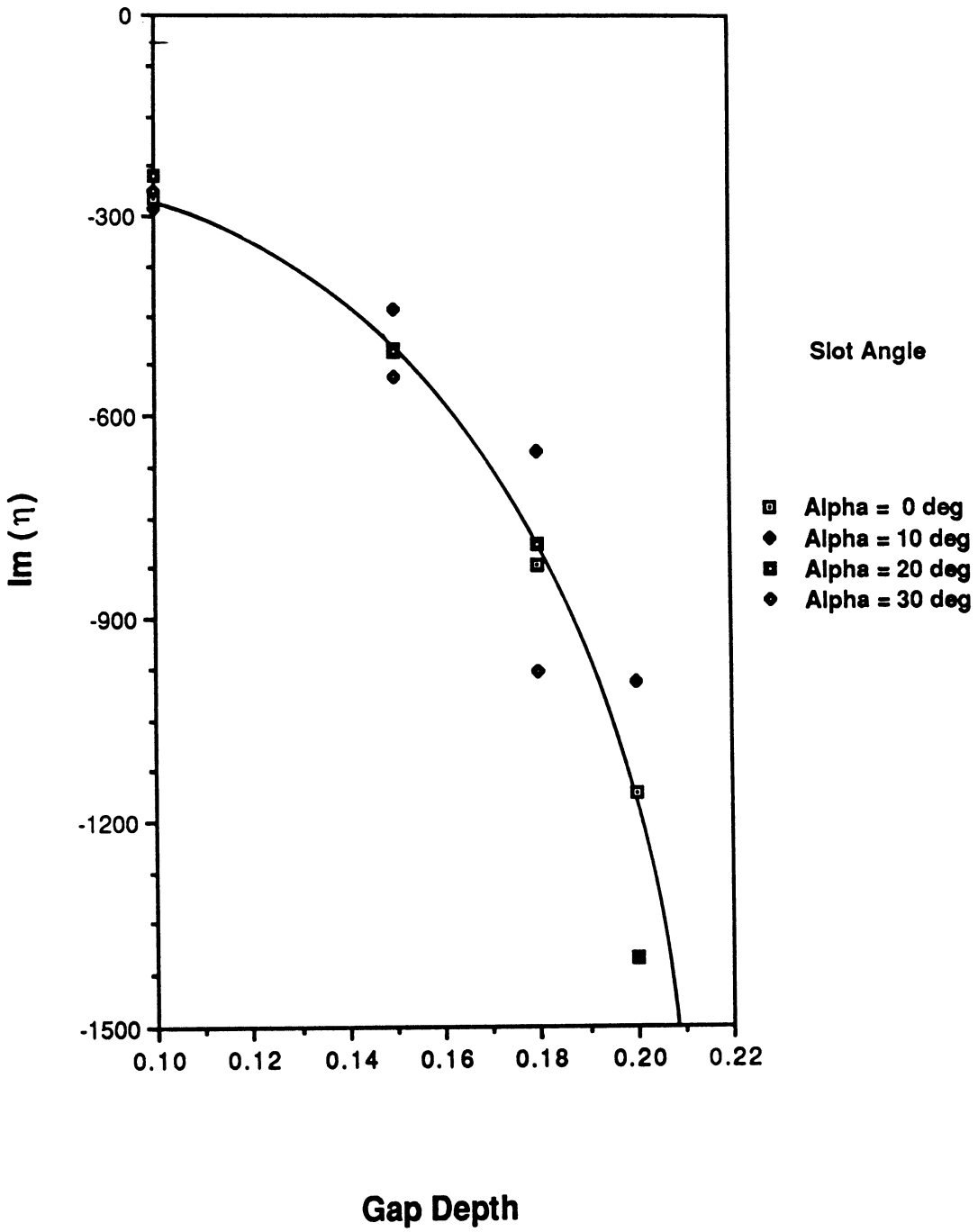

Fig. A-15: Shorted slanted cavities for w = 0.3λ, H-polarization

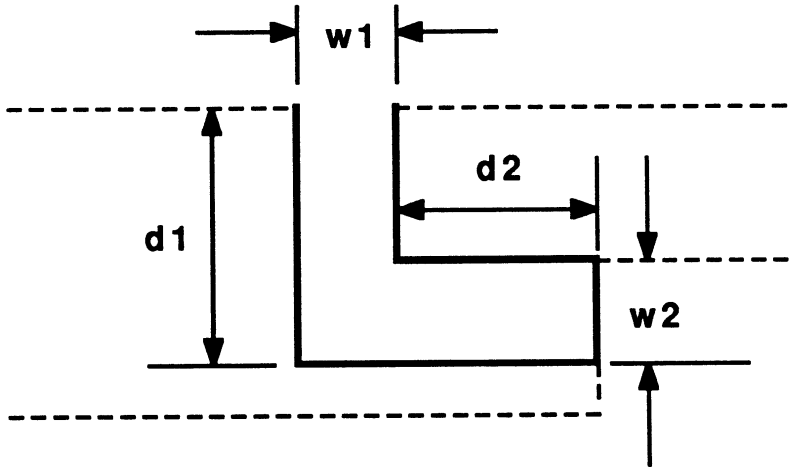

w1	d1	w2	d2	(44)	Num
0.2	0.3	0.1	0.1	+i1160	+i540
0.2	0.3	0.1	.05	+i1160	+i750
0.2	.25	0.1	0.1	+i ∞	-i3118
0.2	.25	0.1	.05	+i ∞	-i2504

Fig. A-16: Results for the shorted cavity shown, H-polarization

Appendix B: Impedance Gap in an Impedance Plane

The key to the success of the preceding formulation is the conversion of an integral over the entire plane y = 0 to one over the surface of the insert or gap alone. This is certainly possible for a resistive insert in a perfectly conducting plane since there is a Babinet principle for resistive sheets [3], but the existance of such a principle is not necessary to reduce the range of integration. This is evident from the fact that we were able to treat an impedance insert (there is no Babinet principle for impedance surfaces), and the reduction can always be carried out by using the Green's function appropriate to the rest of the surface y = 0.

Let us now consider the case of an impedance insert in an impedance plane and, for simplicity, assume the incident field is H-polarized with $\bar{H}^i$ as given in (1). The boundary conditions on y = 0 are then

$$\left(\frac{\partial}{\partial y} + ik\Gamma\right) H_z = 0 \tag{B.1}$$

where

$$\Gamma = \begin{cases} \eta/Z & \text{for} \quad |x| < \dfrac{w}{2} \\ \bar{\eta}/Z & \text{for} \quad |x| > \dfrac{w}{2} \end{cases}$$

and η, $\bar{\eta}$ are the respective surface impedances. Let G(x,y; x',y') be the Green's function for the half-space y ≥ 0 when the entire surface y = 0 has impedance $\bar{\eta}$. If $\bar{\eta} = 0$ or ∞

$$G = \frac{i}{4}\left\{H_o^{(1)}\left(k\sqrt{(x-x')^2 + (y-y')^2}\right) \pm H_o^{(1)}\left(k\sqrt{(x-x')^2 + (y+y')^2}\right)\right\} \tag{B.2}$$

with the upper (lower) sign for $\bar{\eta} = 0$ (∞), but for other values of $\bar{\eta}$, G is given by a Sommerfeld integral. With G defined in this manner, application of Green's theorem to the half-space $y \geq 0$ shows

$$H_z(x,y) = e^{-ik(x\cos\phi_o + y\sin\phi_o)} - \frac{\bar{\eta} - \sin\phi_o}{\bar{\eta} + \sin\phi_o} e^{-ik(x\cos\phi_o - y\sin\phi_o)}$$

$$+ \int_{-\frac{w}{2}}^{\frac{w}{2}} \left(H_z \frac{\partial G}{\partial y'} - G \frac{\partial H_z}{\partial y'} \right) dx' \quad . \qquad \text{(B.3)}$$

The first two terms on the right hand side are the incident and reflected plane waves comprising the total field if there were no insert, and the additional effect of the insert is therefore represented by the term

$$\int_{-\frac{w}{2}}^{\frac{w}{2}} \left(H_z \frac{\partial G}{\partial y'} - G \frac{\partial H_z}{\partial y'} \right) dx' = \frac{ik}{Z}(\eta - \bar{\eta}) \int_{-\frac{w}{2}}^{\frac{w}{2}} H_z\, G\, dx' \qquad \text{(B.4)}$$

which clearly vanishes if $\eta = \bar{\eta}$.

Equation (B.3) can be used to construct an integral equation for H_z in the gap, and one such equation which is analogous to (3) is

$$H_z(x,o) = \frac{2\sin\phi_o}{\bar{\eta} + \sin\phi_o} e^{-ikx\cos\phi_o} + \frac{ik}{Z}(\eta - \bar{\eta}) \int_{-\frac{w}{2}}^{\frac{w}{2}} H_z(x',o)\, G(x,o;x',o)\, dx' \qquad \text{(B.5)}$$

for $|x| < \frac{w}{2}$. For sufficiently small kw with $\bar{\eta}$ finite,

$$G(x,o;x',o) \approx \frac{i}{2} H_o^{(1)}(k|x-x'|) \tag{B.6}$$

and hence

$$H_z(x,o) = \frac{2\sin\phi_o}{\bar{\eta} + \sin\phi_o} e^{-ikx\cos\phi_o} - \frac{k}{2Z}(\eta - \bar{\eta}) \int_{-\frac{w}{2}}^{\frac{w}{2}} H_z(x',o)\, H_o^{(1)}(k|x-x'|)\, dx' \tag{B.7}$$

which can be reduced to

$$-\frac{i}{2}\int_{-1}^{1} J_1(\zeta')\, H_o^{(1)}\left(\frac{kw}{2}|\zeta - \zeta'|\right) d\zeta' = e^{-i\frac{kw}{2}\zeta\cos\phi_o} + a\, J_1(\zeta) \tag{B.8}$$

(c.f (7)) where

$$J_1(\zeta) = \frac{ikw}{2}\,\frac{\eta - \bar{\eta}}{Z}\,\frac{\bar{\eta} + \sin\phi_o}{2\sin\phi_o} H_z \tag{B.9}$$

and

$$a = \frac{2i}{kw}\,\frac{Z}{\bar{\eta} - \eta}\ . \tag{B.10}$$

In terms of $J_1(\zeta)$

$$P_H(\phi,\phi_o) = \frac{i}{2}\,\frac{\sin\phi_o}{\bar{\eta} + \sin\phi_o}\int_{-1}^{1} J_1(\zeta')\, e^{-i\frac{kw}{2}\zeta'\cos\phi}\, d\zeta'\ . \tag{B.11}$$

As in Section 2.1 the final simplification for $kw << 1$ is to write

$$J_1(\zeta) = \left\{1 + \frac{2i}{\pi} A\, P_H(\phi,\phi_o)\right\} J_2(\zeta)$$

where $J_2(\zeta)$ satisfies the integral equation (14) and A is given in (11), and the expression for $P_H(\phi,\phi_o)$ is then

$$P_H(\phi,\phi_o) = \frac{i}{2}\,\frac{\sin\phi_o}{\bar{\eta} + \sin\phi_o}\left\{1 + \frac{\sin\phi_o}{\bar{\eta} + \sin\phi_o}\,\frac{A}{\pi}\int_{-1}^{1} J_2(\zeta')\, d\zeta'\right\}^{-1} \int_{-1}^{1} J_2(\zeta')\, d\zeta'\ . \tag{B.12}$$

In contrast to (15), the diffraction coefficient is a function of ϕ_o for all $\bar{\eta} \neq 0$, but the important thing to notice is that the integral equation for $J_2(\zeta)$ is identical to that for an impedance insert in a perfectly conducting plane apart from a redefinition of the constant a in terms of the difference between the surface impedances of the insert and the surrounding plane. The results in Section 3 of the report now carry over immediately.

The validity of the above approximations is still to be tested and no studies analogous to those shown in Figs. 3 through 8 have yet been made. It is, indeed, possible that a better approximation to the Green's function must be used, and this should be explored. Though we have concentrated on the case of H-polarization, the results for E-polarization follow in principle at least on replacing η/Z and $\bar{\eta}/Z$ by Z/η and $Z/\bar{\eta}$ respectively, but the accuracy of the approximations will then improve as η and $\bar{\eta}$ increase rather than decrease.